Empirical Prediction of Optimum Process Conditions of Spark Plasma-sintered Magnesium Composite (AZ91D-Ni-GNPs) using Response Surface Methodology (RSM) Approach

Olugbenga Ogunbiyi*, Samuel A. Iwarere*, Michael O. Daramola

Department of Chemical Engineering, Faculty of Engineering, Built Environment and Information Technology, University of Pretoria, Hatfield 0028, Pretoria, South Africa.

*Corresponding Author: olugbengaogunbiyi@gmail.com, samuel.iwarere@up.ac.za (orcid:0000-0001-8566-6773)

Abstract

In the present study, nickel (Ni) and graphene nanoplatelets (GNPs) are considered as ideal reinforcements for Mg-9Al-1Zn (AZ91D) magnesium alloy to form metal matrix composites (MMCs) because of their excellent mechanical properties. It is essential to utilize effective manufacturing techniques to develop AZ91D magnesium (Mg) alloy-nickel-graphene nanoplatelets (AZ91Z-Ni-GNPs) MMCs. Hence, the spark plasma sintering method is used to fabricate AZ91D-Ni-GNPs composites. HRTEM, OM, SEM, EDS, XRD, and Raman spectroscopy were used to investigate the microstructure, crystallinity, and elemental composition of both the blended powder and the sintered composites. GNPs and Ni were well-dispersed in the AZ91D Mg matrix, and effective interfacial bonding is formed between GNPs, Ni, and Mg alloy matrix powder before sintering. A Response Surface Methodology (RSM) with a central composite design was used to design the experiments by considering two variables, i.e., sintering temperature and pressure. The method was adopted to eliminate the trial-by-error approach. Using the data generated, quadratic regression models were developed for the relative density (g/cm^3), and Vickers hardness (HV) of the MMCs, and the parametric effects were explained via RSM. The process parameters were optimized, and the effective interaction between two descriptive variables (process parameters) on the relative density, hardness, and microstructural properties of Mg-based composites was investigated. Validation of the experimental run was performed using optimal process parameters acquired from the analyses to demonstrate the enhancement in the properties of the sintered composites. It was observed that the sintering temperature had a major influence on the relative density and hardness properties (responses). The optimal relative density and hardness obtained for AZ91D-Ni-GNPs composites were 1.723 g/cm^3 and 93.21 HV, respectively. The addition of GNPs to AZ91D-Ni produced material with improved properties.

Keywords: RSM; Magnesium composites; AZ91D-Ni-GNPs; GNPs; Density; Hardness; Empirical modelling

1. Introduction

The continuous demand for lightweight advanced materials with improved mechanical properties to replace conventional heavy-weight materials has increased in recent years. Magnesium (Mg)

and its alloys are a suitable substitute for aluminium, and they have been in high demand for different engineering applications in automobile, construction, aerospace, and biomedical industries because of their low densities [1, 2]. Their densities are ~35% lighter than aluminium, ~80% lighter than nickel, ~75% lighter than steel, and ~60% lighter than titanium [3]. The prevalent applications of magnesium alloys are connected to their unique properties, such as high specific strength, good thermal conductivity, dimensional stability, excellent machinability, and good castability. Specifically, in the automobiles industry, lightweight and strong magnesium alloys/composites help in saving fuel consumption and improve efficiency [4]. Nevertheless, limitations such as low hardness, poor ductility, wear resistance, corrosion resistance, and tensile strength have hindered their extensive applications in the industries that require materials with high ductility and strength [5]. While Mg alloys are used in automobiles (seat frames, engine blocks, steering wheel frames, etc.) and electronic industries (because of their damping and electromagnetic shielding ability, which reduce noise), they have limited applications in wet areas due to poor strength, wear, and corrosion resistance properties [6]. Thus, several studies have been conducted to formulate Mg-based materials with good strength and tribological properties (less reactive to wear and frictional failure).

Based on the above reasons, different reinforcement materials have been introduced to monolithic Mg matrix and Mg alloys matrices to obtain magnesium matrix composites with improved microstructure and good mechanical properties. Materials such as metals (Ni, Ti, Si, and Al) [4, 7, 8], ceramic compound (Si_3N_4, AlN, Al_2O_3, TiN, and TrB_2, to mention a few) [9], and carbonaceous (carbon nanotube (CNT) and graphene) materials have been used as reinforcements [10-12]. For instance, powder silicon (Si) particles at different percentage compositions were used to reinforce Mg alloy, and the result shows that the tribology properties were improved [13]. Furthermore, graphene (carbonaceous nanomaterials) as reinforcements have been used either in place of ceramic particles such as Si_3N_4, AlN, Al_2O_3, TiN, TrB_2, etc., or as a hybrid reinforcement. There are different types of graphene such as graphene nanoribbons, nanoparticles, nano-sheets, nanoplatelets, and 3D graphene [14]. Graphene generally possesses high thermal conductivity of 5000 $Wm^{-1}K^{-1}$, excellent tensile strength of 130 GPa, charge carrier mobility of 200 000 $cm^2 V^{-1}s^{-1}$, high elastic modulus of 1 TPa, low coefficient of thermal expansion, excellent self-lubrication, and good damping capacity properties [15, 16]. Hence, these properties have positioned graphene as an ideal reinforcement for improving the mechanical and tribological properties of metal matrices such as Mg alloys. Graphene nanoplatelets (GNPs) belong to the carbonaceous nanomaterials group, utilized in many structural applications. Its structural formation is widely documented in the literature [17, 18]. Similarly, graphene dispersibility in metal matrices is better compared to tubular CNTs because of its characteristic two-dimensional (2D) sheet-like morphology [19].

In the tribology testing of GNPs-reinforced metal composites, the report shows that a continuous layer of solid lubricant was formed on the surface of reinforced metal composites [20]. This happened because of the good dispersion of GNPs leading to the efficient contribution of self-

lubricant characteristics to the oxide tribo-layer and thus, producing an effective decrease in the wear rate and coefficient of friction properties of the composite (sliding of GNPs-reinforced metal composite against a counterface of H13 alloy tool steel) [20]. GNP is not a perfect material due to the presence of structural defects such as cracked edges and wrinkles. However, they are beneficial in strengthening the grain boundaries (strengthening the interface between GNPs and Mg matrix) and forming strong metallurgical bonding [21, 22]. In the reinforcement of Mg alloy using GNPs, the carbon atoms present in GNPs interact with the Mg atoms to impede dislocation movement during plastic deformation, thereby increasing the yield strength and hardness property [22, 23]. Beyond the contribution of GNPs in improving the microstructure and mechanical properties of Mg alloys, the selection of good fabrication techniques and suitable combinations of process parameters significantly influence the physical and mechanical properties of materials. Consequently, Mg-based alloys and composites have been manufactured using various methods; melt infiltration, stir casting, disintegrated metal deposition, powder metallurgy (PM), etc. Also, several studies have reported the beneficial effect of using PM methods in the manufacturing of metal alloys and composites [24, 25].

PM is an advanced metal manufacturing technology utilized to produce high-quality structural components to its near-net-shape [25]. Comparably, many researchers have applied different PM technology to fabricate Mg alloys/composites [25, 26]. In two separate studies, the possibilities of manufacturing Mg-based composites using different PM methods were demonstrated. Firstly, Wong and Gupta [27] manufactured magnesium composites (copper particulates reinforced Mg) using microwave-assisted two-directional sintering PM. Secondly, Fukuda et al. [28] manufactured AZ61 magnesium-based composites (carbon nanotube reinforced AZ61 alloy) using PM wet processing technique. Among PM methods, spark plasma sintering (SPS) is a promising method used to develop metal alloys and composites because it is faster, cleaner, and offers reduced structural defects (porosity, segregation) [29, 30]. It is a processing route that is beneficial in developing bulk components because high temperature is generated locally with a fast-heating rate between powder particles leading to densification. A pulse electric current is generated and flows directly in the sintered materials creating plasma at the contact point between the particles, thus aiding densification. In the process, high heating efficiency leads to the high-quality sintered component achieved at a lower sintering temperature within a short time compared to the conventional sintering process [31-33]. In the study of Song et al. [34], magnesium-based composites were manufactured by SPS. The results indicated that the SPS played a significant role in enhancing the hydrogen storage properties of magnesium-based composites. The mechanism of operation and benefits of using SPS in metal forming have been widely reported in the literature [30, 35].

It is noteworthy that using the wrong combinations of process parameters: sintering temperature, heating rate, pressure, and soaking time could result in poor densification and mechanical properties. Thus, Response Surface Methodology (RSM), among other statistical and mathematical tools, is a design of experiments method used to design experimentations within the

controlled intervals in order to find the complex relationship between the preferred input variables and responses [36]. It offers several advantages such as reducing the number of experimentations, level of independent variables, cost of operation, and presenting internal estimations of errors [37, 38]. To a large extent, RSM has been used to effectively optimize the relationship between the input variables and the expected response for different alloy and metal composite systems (A413 alloy [39], Cu-Zn alloy [40], PVP-B-Hf composites [41], and so on). In order to minimize errors in the combination of suitable process parameters and to avoid a trial-and-error approach in the manufacturing of graphene nanoplatelets/nickel reinforce Mg alloy, this study employs RSM to recognize the significance of input variables, especially the sintering temperature and pressure with the expected response; density and hardness. In the process, quantitative relationships between the input variables, the optimum experimental parameters, and optimal microstructure, including the phases developed, were analyzed in detail.

2. Materials and method

2.1. Materials

The gas atomized Mg-9Al-1Zn (AZ91D) Mg powder supplied by Dome metal China is used as the matrix material. The nickel powder provided by Wear tech Ltd, South Africa, and graphene nanoplatelet supplied by Sigma-Aldrich, South Africa, were used as reinforcement. The AZ91D Mg alloy has a 99.7% purity with a spherical particles size range of 15 - 53 μm. Nickel has a 99.5% purity with a spherical particles size range of 0.5 – 3 μm. Graphene nanoparticles (GNP) have an average diameter size of 5 μm, an average thickness of 15 nm, and a surface area of 50 – 80 m^2/g. **Table 1** shows the weight percentage chemical composition of the as-received matrix and reinforcement powder coupled with the particle's sizes, as indicated by the supplier.

Table 1. Percentage weight of AZ91D-Ni-GNPs Mg-based composite

Element	AZ91D	Ni	GNP
W%	97	1.5	1.5
Particle size (μm)	15 - 53	0.5 - 3	0.015

2.2. Powder preparation

According to the design of the experiment, the matrix powder and the reinforcing powders were carefully measured using a digital weighing balance. The measured powders were poured into a plastic container and then placed in a tubular mixer. The tubular mixer holding chamber moves in a 3D direction (combining translational and rotational motion). A tungsten ball at a ratio of 10:1 ball to powder is added to the powders to ensure thorough mixing in a dry environment. The mixing speed was set at 110 rpm for 10 h. Afterward, the admixed powder is transferred to a planetary ball milling machine (PM 400) to ensure systematic mechanical alloying. The mixing is done in a wet environment containing ethanol solution and tungsten balls, added at a ratio of 10:1 to promote

homogenization. The airtight alloying process is performed for 5 h, with a speed of 200 rpm [4]. After the alloying cycle, the wet powder is transferred to a LAB conco vacuum dryer and dried at 70 ℃ for 6 h. The description of the milling machine and its operating procedure is reported in our previous study [15]. At the end of the drying process, the powders with the tungsten balls were transferred into the tubular mixer to ensure blending for 1 hour. It is operated at a very low rotating speed of 49 rpm to eliminate any form of agglomerate that might have developed during drying. A 5.43 g admixed powder is measured into the prepared mould and placed in the furnace chamber of the SPS machine to develop a θ20 mm by 10 mm sintered component.

2.3. Spark Plasma Sintering

A spark plasma sintering equipment from Germany (HHPD-25 FCT system) is used to develop the Mg-based composites. The process parameters were set according to the Design of Experiment (DoE)-RSM developed. The selection of the process parameters utilized in the DoE-RSM is based on a similar study in the literature on the manufacturing of AZ91D Mg powder (matrix) [42, 43]. While the figure reported in the literature served as a guild, preliminary sintering was conducted since the machine is different. It was discovered that a temperature of around 500 ℃ at a heating rate of 100 ℃/min with 50 MPa pressure is sufficient to obtain high densification close to the theoretical density (1.69 g/cm^3 densification was obtained which is 96%). The preliminary experiment guild in the DOE design for this study. The sintering temperatures were set between 450 and 500 ℃, a pressure between 30 - 50 MPa, a heating rate of 100 ℃/min, and a soaking time of 5 min. The vacuum atmosphere in the heating chamber was preserved at 0.5 mbar using argon in order to reduce oxygen contamination to the barest minimum. The theoretical density of the mixed powder is calculated to be 1.76 g/cm^3. Prior to sintering, the graphite mould (graphite die and punches) was prepared using 0.2 mm thick graphite paper to line the inner surface of the graphite die. This is necessary to aid heat distribution and ensure easy removal of the sintered sample at the completion of the sintering cycle. A disc size of 20 mm diameter by 10 mm height was sintered for all the samples using 5.43 g composite powder for each sample. The sintering was completed quickly, and the machine switched off. The sample was allowed to cool in the furnace before removal: a process that was repeated for all the samples. At the end of the sintering cycle, the samples were sandblasted to remove unwanted impurities such as carbon film deposited on the surfaces of the fabricated samples. The impurities were as a result of graphite paper utilized in the mould [44]. The schematic image of the SPS manufacturing setup and the preparation of AZ91D-Ni-GNPs magnesium composites is shown in **Figures 1 and 2.**

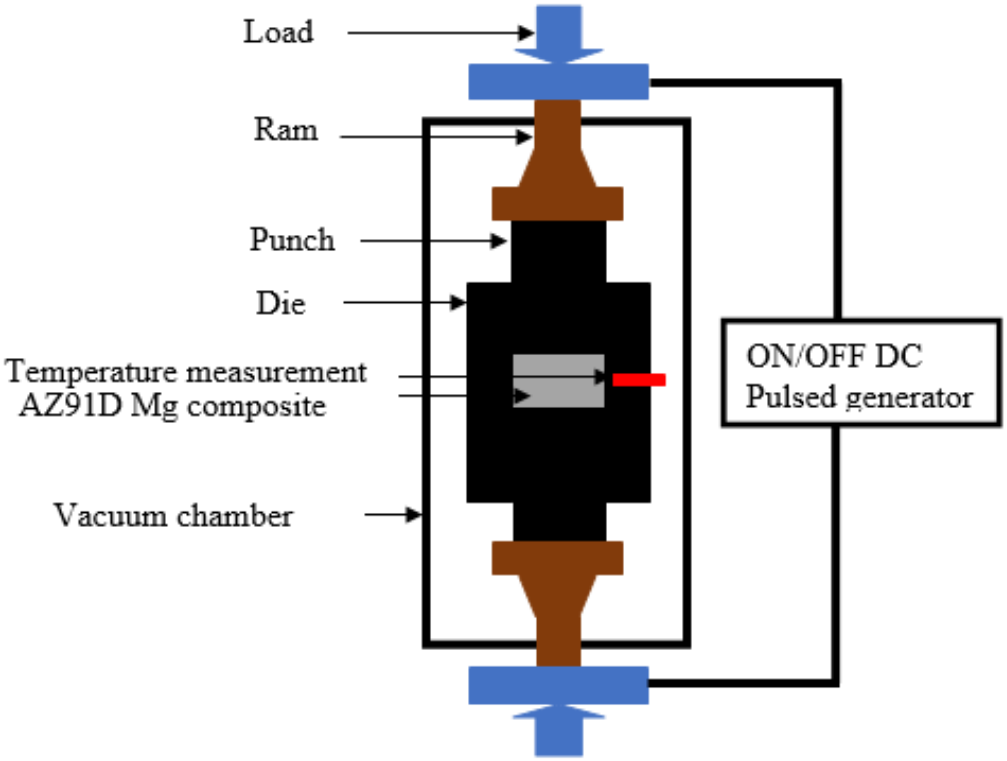

Figure 1. Schematic diagram of SPS powder consolidation setup

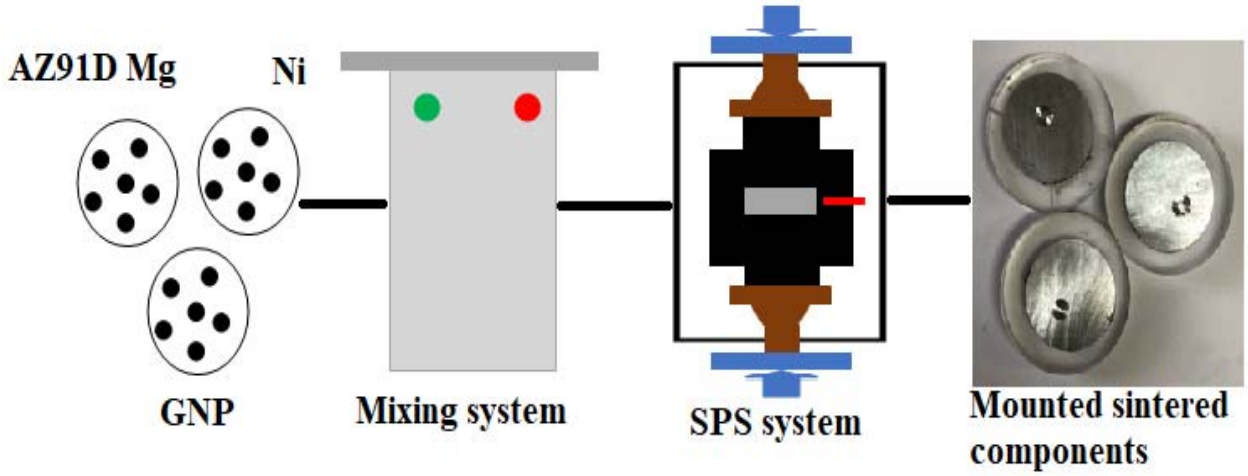

Figure 2. Manufacturing steps for producing AZ91D-Ni-GNPs magnesium-based composites

2.4. Density and microhardness measurement

The experimental relative density of the sintered Mg-based composites was estimated following the Archimedes method [45] using an electronic digital weighing balance with an accuracy of ± 0.0001g. Furthermore, the relative density in percentage was calculated using simple mathematical arithmetic in equation 1.

$$\frac{ED}{TD} \times 100 \quad (1)$$

Where ED and TD are the experimental density and theoretical density.

It was ensured that the test was repeated 6 times and the average calculated to represent the actual observed density of the sintered component. The theoretical density was calculated by using a simple arithmetic rule [46]. The microhardness values of the sintered Mg-based composites were investigated using a Vickers microhardness (HV) tester (Future-tech, 800) machine. The testing parameters used were a load of 100 g/f, a dwell time of 20 s, and a spacing of 0.1 (conducted at room temperature). The prepared surface of each sample was indented 6 times at 6 different positions to ensure that all features present were represented and to ensure data accuracy. The average of 6 indentions data obtained was calculated and taken as the actual microhardness value of the sintered composites. This is repeated for all the samples.

2.5. Experimental design and data collection

2.5.1. Experimental design

In this study, the DoE-RSM ease is utilized to optimize the process parameters in SPS manufacturing to establish a high-quality sintered component that possesses the highest microhardness and density. The quadratic regression equation in the RSM model is shown in equation 2 and written as follows [2]:

$$A = \beta_O + \sum_{i=1}^{k} \beta_i x_i + \sum_{i=1}^{n} \beta_{ii} x_i^2 \sum_{i<j} \beta_{ij} x_i x_j + \varepsilon \quad (2)$$

Where A represent either the density or hardness of the sintered components, x_i and x_j represents the combination of process parameters: the sintering temperature and pressure. $x_i x_j$ and x_i^2 are the interactive effects and secondary independent variables. The linear, quadratic, and regression coefficients are β_i, β_{ii} and β_{ij} while β_O is a constant. The random error is ε and k represent the number of variables considered which is presented in equation 3 as:

$$N = 2k\,(k - 1) + C_P \quad (3)$$

Where N represent the total number of experiments and C_P represent the number of central points.

In the sintering process, the sintering temperature and pressure represent the factors considered to affect the density and hardness of the sintered components. The factors have a low-level value set at 450 ℃ and 30 MPa for temperature and pressure, a medium level value set at 480 ℃ and 40 MPa, and a high-level value of 500 ℃ and 50 MPa sintering temperature and pressure, respectively. To effectively analyze the influence of various factors on the density and hardness properties of the sintered components, the sintering temperature and pressure range were narrow between 450 to 500 and 30 to 50 MPa, respectively. **Table 2** shows the symbols, levels, and values used in the RSM design of spark plasma sintered Mg-based composites.

Table 2: Independent variables (factors: symbols, level, and values) in the RSM of spark plasma sintered Mg-based composites.

Symbols	Variables	Levels		
		-1	0	1
A	Temperature (℃)	450	480	500
B	Pressure (MPa)	30	40	50

2.6. Microstructure characterization and measurement

The sectioned samples were metallographically prepared using different grit sizes of silicon carbide papers from 320 to 4000 to remove rough surfaces and scratches. A diamond paste (diamaxx: mono 6 and 3 μm) and alumina powder were used for the polishing. The microstructures and morphologies of the sintered AZ91D-Ni-GNPs were assessed via optical microscope (Falcon 500 series) and field emission scanning electron microscopy (FE-SEM) incorporated with an EDS detector suite INCA X-Stream 2 pulse analyzer software (Zeiss Ultra Plus 55). It was operated at 2.0 kV with 70 s acquisition time. The morphology of the admixed powder of the Mg-based sintered composites was assessed via high-resolution transmission electron microscopy (HR-TEM) JEOL 2100 (FROM Tokyo, Japan). It was equipped with a Gartan U1000 camera 0f 2028 x 2028 pixels operated at 200 kV. The optical micrographs obtained showing different grain shapes and boundaries were evaluated by measuring the area of the grains in each direction to understand the grain size distribution. ImageJ graphics software was used for this purpose on each optical micrograph. The phases present were investigated via a PANalytical Empyrean x-ray diffraction (XRD) machine with a reflection geometry value of 2θ = 5 - 90° and a step size of 0.01° activating with a CuKα radiation source (λ = 0.178901 nm). A Confocal micro-Raman spectrometer (Alpha 300 RAS: WiTec Focus Innovations, Germany) position at 532 nm laser wavelength was utilized to characterize the sintered Mg-based composites. A laser power of 5 mW and 150 s spectral acquisition time was used for the measurement.

2.7. Model development, validation, and analysis of variance

The variance (ANOVA) analysis is performed on the modified models as estimated by the statistical tool. The statistical tool is utilized to analyze the F test (for F and P values), evaluate the effect of the factors, and investigate the interactive effect of variables. In other words, the ANOVA model assists in recognizing the differences in the data acquired and separate into components. This implies that values characteristics are estimated individually and reported in the ANOVA table for all terms that emerge in the model equations [47]. In order to validate the accuracy of the suggested models, various parameters are considered, especially the precision of the predicted values obtained compared to experimental values. Some of the parameters considered include the coefficient of determination (R^2), lack of fit (LOF), adequate precision, adjusted coefficient of

determination (Adjusted R^2), and coefficient of variation (C.V.). More importantly, the major parameters that indicate the correctness of the model and suggest that a model is significant are the R^2 and Adjusted R^2. In addition, the p-value of a model should be < 0.05, and the F value should be large (> unity) for a model to be considered significant [2].

In this study, the R^2 values obtained were closer to 1, indicating that the experimental results and the estimated results are in satisfactory agreement within the range of the experiment. The coefficient of variant (C.V) is used to quantify the residual variability in the data as a percentage of the mean of the response variable. The repeated experimental design points present the "residual error" and "Pure Error," which are compared using the Lack of Fit (LOF) parameters. The 3D mapping is utilized to evaluate the effect of individual variable independently and their interactions on the acquired responses. Thus, the sequential process for developing the model using Response Surface Methodology is shown in **Figure 3**.

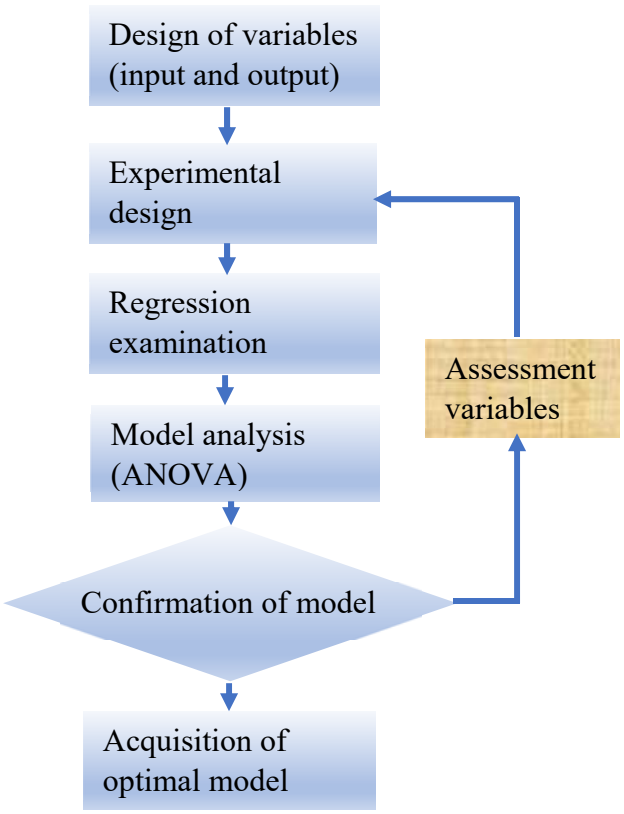

Figure 3. The process of the model developed using the Response Surface Methodology

Following this process, regression analysis using backward elimination was executed to accurately obtain the model prediction for relative density and hardness properties of AZ91D-Ni-GNPs composites. An ~95% confidence level for the models was achieved from the ANOVA analyses of relative density and hardness properties.

3. Results and discussion

3.1. Characterization of AZ91D-Ni-GNPs powder and GNPs

Figure 4 shows the SEM and TEM micrographs of the admixed composite and GNP powders. In addition, **Figure 5** shows the elemental dispersion (EDS) and percentage constituents present in the admixed composite powder. The graphene nanoplatelets (GNPs) powder from the SEM micrograph revealed that the particles form an irregular shape with wrinkle sheets of different dimensions. The AZ91D-Ni-GNPs powder was analyzed with SEM/TEM. The SEM image could not reveal the presence of GNPs due to the low percentage of constituents added. However, the TEM revealed the presence of GNPs positioned between the matrix particles. The SEM-EDS mapping shows the presence and distribution of the major elements in the composites. The EDS revealed that some of the particles of GNP adhered to the surface of matrix particles while few others were present between the particles. This suggests that the thin layers and wrinkled GNPs form a shell and cover the surfaces of the matrix particles, thereby having an effective reinforcing influence on the composites. The Ni constituent is sparsely distributed, resulting from the low quantity used as reinforcement (1.5%). Other constituents such as Al, Mn, and Zn are the primary trace elements visible from the SEM-EDS analysis, which is a typical characteristic of AZ91D magnesium grade [48].

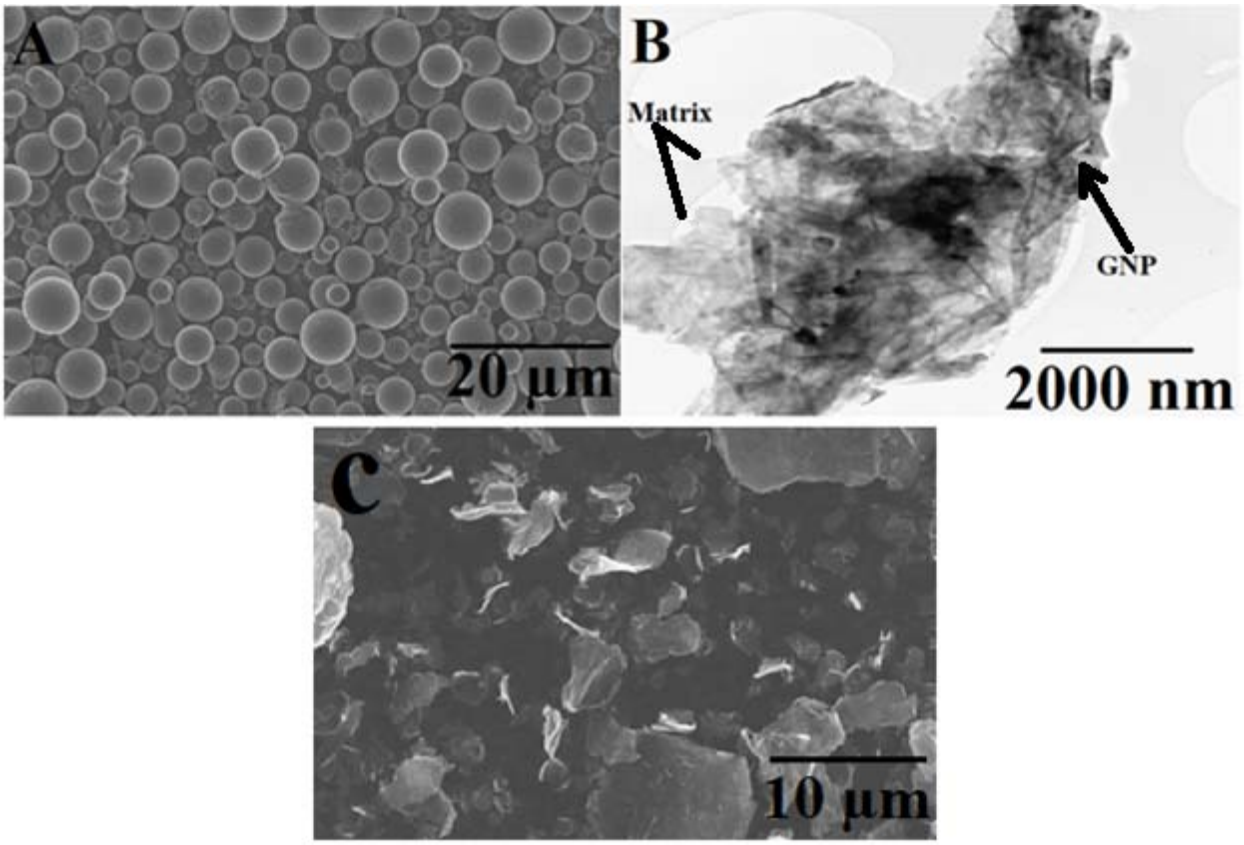

Figure 4. (a) SEM micrograph of AD91Z-Ni-GNPs composite powder (b) TEM micrograph of AD91Z-Ni-GNPs composite powder and, (c) SEM micrograph of GNPs powder

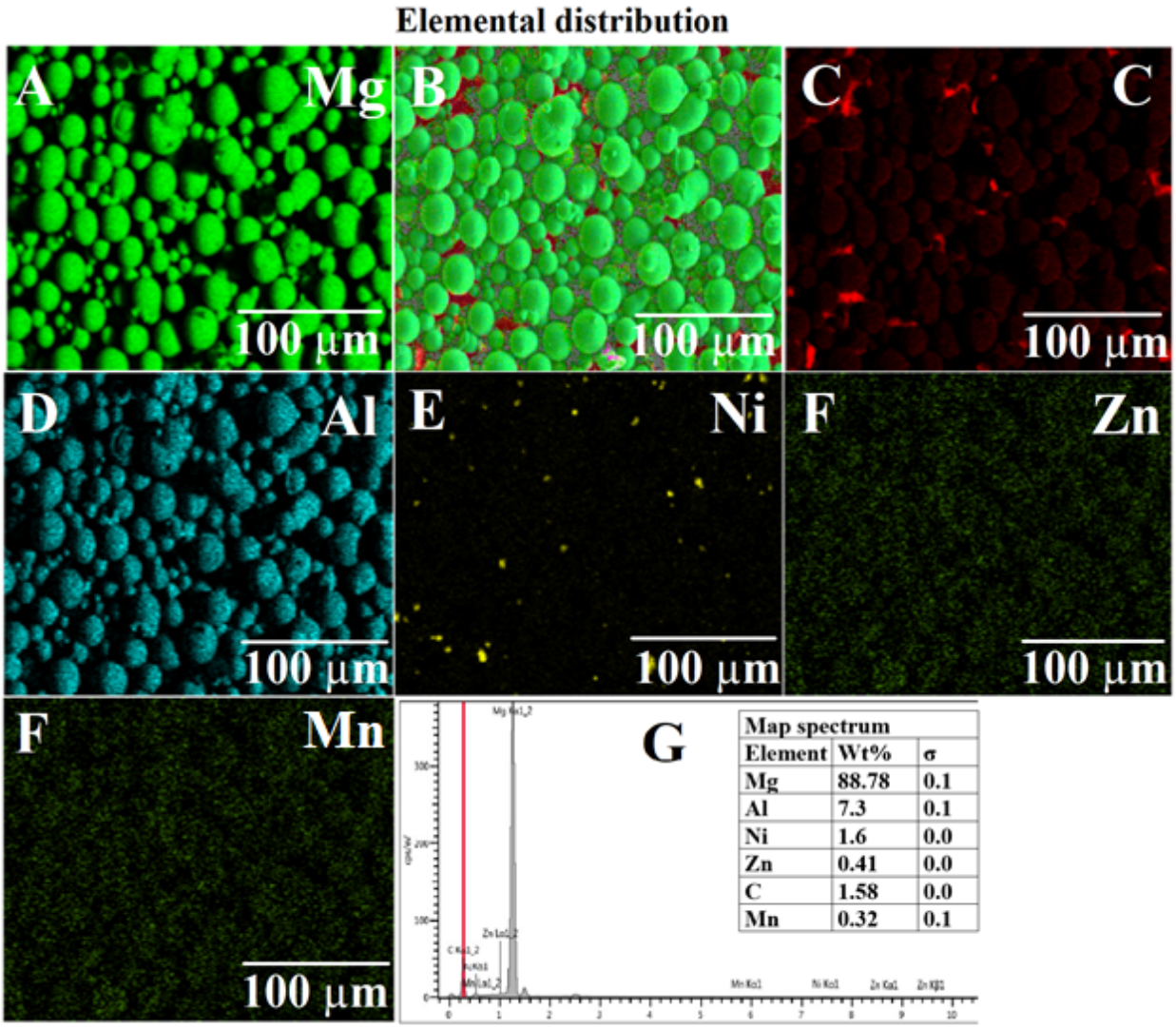

Figure 5. Elemental distribution mapping of AZ91D-Ni-GNPs Mg-based composite. (a) Magnesium matrix, (b) Combine colour mapping, (c-f) C, Al, Ni, Zn, and Mn distribution, and (g) EDS analysis.

3.2. Model development and validation

The experiment was designed using the central composite design using two factors: the sintering temperature and pressure with the responses being relative density and hardness. These are shown in **Table 3**. The sintering temperature is set between 450 - 500 ℃. This temperature range is selected based on the result obtained from the preliminary study conducted, which indicates that a higher sintering temperature above 500 ℃ results in melting the AZ91D-Ni-GNPs powder out of the mould. The melting temperature provided by the manufacturer of AZ91D magnesium in the data-sheet is 651 ℃. The sintering temperature used conforms with a similar study conducted by Dikai G. et al. [49], where AZ31 magnesium was cryomilled before sintering using the SPS method. In addition, a sintering temperature below the range of temperature selected results in low

consolidation and densification of the sintered component. The use of high sintering temperature close to the melting temperature of matrix powder, high pressure, and nanoparticle reinforcement result in the formation of strong metallurgical bonding between the matrix and reinforcement [2]. Thus, the strong adhesion present in the structure of the composites (bond formation) as a result of diffusion at high temperature in the sintered component results in good densification and high hardness property.

Table 3. Designed matrix and experimental results with the residual error for AZ91D-Ni-GNPs magnesium-based composites.

Run	Factors		Responses					
	Temperature A (℃)	Pressure B (MPa)	Actual relative density (g/cm^3)	Predicted relative density (g/cm^3)	Residual error for relative density	Actual hardness (HV)	Predicted hardness (HV)	Residual error for hardness
1	480	40	1.6920	1.6924	-0.0004	74.62	73.88	0.7438
2	500	30	1.6590	1.6591	-0.0001	48.58	46.65	1.9300
3	480	40	1.6920	1.6924	-0.0004	74.62	73.88	0.7438
4	480	40	1.6920	1.6924	-0.0004	74.62	73.88	0.7438
5	450	50	1.7230	1.7237	-0.0007	93.21	93.36	-0.1468
6	480	50	1.7040	1.7065	0.0025	82.89	85.13	-2.2400
7	450	30	1.7010	1.7006	0.0004	68.76	69.21	-0.4521
8	480	40	1.6920	1.6924	-0.0004	74.62	73.88	0.7438
9	450	40	1.7190	1.7187	0.0003	83.27	82.67	0.5989
10	500	40	1.6710	1.6690	0.0020	56.74	61.06	-4.3200
11	480	30	1.6850	1.6853	-0.0003	58.37	59.85	-1.4800
12	480	40	1.6920	1.6924	-0.0004	74.62	73.88	0.7438
13	500	50	1.6940	1.6958	-0.0018	75.08	72.69	2.3900

3.3. The response surface methodology of the two responses

The degree of interaction of the two factors on the mechanical properties of the sintered composites was examined using central composites design (CCD) of the RSM. This is further clarified by analyzing the statistical model of the results produced from the ANOVA obtained, comparing the hardness and density as a function of the neutral process variables (responses). Similarly, the

regression provides information on the accuracy of the data obtained and the relationship between the factors and responses. In confirming the significance of different model coefficients, the importance of the regression model and the lack of fit are essential to ascertain the correctness of the model and the predictive ability. Therefore, the statistical parameters of the model equations obtained and the confirmation of the results in the ANOVA models for density and hardness are summarized in **Tables 4 - 7,** respectively.

3.4. Development of the prediction models, analysis of the ANOVA, and fitting of the model of density and hardness measurement for the sintered AZ91D-Ni-GNPs composites

The significance and ANOVA test from the response surface model were determined to summarize the results of the prediction models for density and hardness presented in **Table 4 - 7**. From the tables, the F-values for the density and hardness are 318.57 and 60.78, respectively, combined with the P-values that are less than 0.05 for the density and hardness. This is an indication that the models are statistically significant, which means that the probability of having a "model F-values" with a high magnitude because of noise is only 0.01%. Similarly, the small values of P for the two models show that the corresponding coefficient is very significant, thus contributing immensely to the response variables. However, a P-value greater than 0.100 signifies that the model terms are insignificant. For the ANOVA model of density measurement, all the factors terms are significant (A, B, AB, $A^{2,}$ and B^2). In contrast, only three factors terms are significant (A, B, and A^2) in the model with the hardness ANOVA. The factor terms AB and B^2 in the hardness ANOVA model are more than 0.05, indicating that they are not significant terms. The lack of fit assessment for both density and hardness models is within the nonsignificant range in comparison to pure error, suggesting that the model fits appropriately with the data obtained experimentally, thus desirable. The coefficient of variation for the density model is 0.0869%, and hardness is 3.25%, respectively, implying that the difference between the experimental and predicted values is small. In order to declare a model good fit, a value above 0.80 for the determination coefficient (R^2) is required. In this study, the R^2 for both density and hardness models are 0.9956 and 0.9775, respectively, which clearly indicates that they are close to unity. Thus, 99.3% and 97.8% of the total variance in density and hardness measurement is ascribed to the experimentally investigated variables, suggesting that the prediction of the model is suitable for fitting the experimental values.

Nevertheless, a good regression model is not adequate, even with a large value of R^2, because R^2 increases with the addition of variables. Therefore, the Adjusted R^2 is equally crucial as it explains the standard testing for fitting the regression model. The Adjusted R^2 for density and hardness is similarly larger than 0.80 (0.9925 for density and 0.9614 for hardness), implying that the models are adequate with no need to consider adding other terms. The standard deviation of the two models (density and hardness) are 0.0015 and 2.35, respectively. Consequently, the closeness of R^2 values to 1 and the smaller values of standard deviation indicates that the models are good, and there is minimal difference between the predicted values and experimental values (responses). The variation between the adjusted R^2 of 0.9925 and 0.9614 for density and hardness is less than 0.2, indicating that they are in reasonable agreement. A value greater than 4 is desirable to measure the

signal-to-noise ratio using the adequate precision term. This is calculated by dividing the difference between the minimum and maximum predicted response by the average standard deviation value of all the predicted responses. A precision value of 64.5402 and 29.2669 for density and hardness implies that the signal is satisfactory. Thus, the models can be utilized to navigate the design space. A nonlinear correlation was determined between the descriptive variables and response variables. This is the CCD-based quadratic model used to forecast the density and hardness properties of AZ91D-Ni-GNPs composite as a function of A (temperature) and B (pressure) presented in coded factors in **Equation 4 and 5**.

$$\text{Density} = -1.22752 + 0.013863A - 0.011688B + 0.000014AB - 0.000016A^2 + 0.000084B^2 \quad (4)$$

$$\text{Hardness} = -1324.02983 + 6.09918A + 1.46280B + 0.001897AB - 0.006955A^2 - 0.013867B^2 \quad (5)$$

Table 4. ANOVA tests for predicting the quadratic model of the density of AZ91D-GNPs magnesium composite

Source	Sum of Squares	Df	Mean Square	F-Value	P-Value	
Model	0.0035	5	0.0007	318.57	< 0.0001	significant
A-Temperature	0.0018	1	0.0018	831.79	< 0.0001	
B-Pressure	0.0013	1	0.0013	613.97	< 0.0001	
AB	0.0000	1	0.0000	21.47	0.0024	
A^2	0.0002	1	0.0002	113.78	< 0.0001	
B^2	0.0002	1	0.0002	90.59	< 0.0001	
Residual	0.0000	7	0.0000022			
Lack of Fit	0.0000	3	0.0000051			
Pure Error	0.0000	4	0.0000			
Cor Total	0.0035	12				

R^2: 0.9956, Adjusted R^2: 0.9925, Adequate precision: 64.5402

Table 5. Statistical parameters of the quadratic model of the density of AZ91D-GNPs magnesium composite.

Type of variable	
Standard deviation (SD)	0.0015
Coefficient of variation C.V (%)	0.0869
Mean	1.69
R-squared	0.9956
Prediction error (PRESS)	0.0002
Predicted R-squared	0.9663
Adjusted R-squared	0.9925
Adequate precision	64.5402

Table 6. ANOVA tests for predicting the quadratic model of the hardness of AZ91D-GNPs magnesium composite

Source	Sum of Squares	Df	Mean Square	F-Value	P-Value	
Model	1677.06	5	335.41	60.78	< 0.0001	Significant
A-Temperature	700.70	1	700.70	126.98	< 0.0001	
B-Pressure	938.35	1	938.35	170.05	< 0.0001	
AB	0.9120	1	0.9120	0.1653	0.6965	
A^2	47.23	1	47.23	8.56	0.0222	
B^2	5.31	1	5.31	0.9625	0.3592	
Residual	38.22	7	5.52			
Lack of Fit	38.63	3	12.88			
Pure Error	0.0000	4	0.0000			
Cor Total	1715.69	12				

R^2: 0.9775, Adjusted R^2: 0.9614, Adequate precision: 29.2669

Table 7. Statistical parameters of the quadratic model of the hardness of AZ91D-GNPs magnesium composite.

Type of variable	
Standard deviation (SD)	2.35
Coefficient of variation C.V (%)	3.25
Mean	72.31
R-squared	0.9775
Prediction error (PRESS)	271.27
Prediction R-squared	0.8419
Adjusted R-squared	0.9614
Adequate precision	29.2669

3.5. The normal probability plot of residuals for both density and hardness of AZ91D-Ni-GNPs composites

The normal plot of residuals and the correlations between the predicted and actual for the two responses (density and hardness) are shown in **Figures 6a, 6b, 7a,** and **7b,** respectively. The residuals plot explains the difference between the predicted and the observed responses. The differences between the experimental and predicted value are interpreted with the normal probability plot, which explains the adequacy of the model from the data applied. As such, a model that is adequate is the one that has its points connected on a straight line in the normal probability plot of the residual. This could be observed from **Figures 6 (a, b) and 7 (a, b)** for both density and hardness normal probability plots models showing well-aligned residual points. By implication, the errors are not concentrated in a particular section but somewhat random within the error portion, and the residuals are dispersed normally. Also, the errors are minimal because the residuals in the normal plots for density and hardness are close to the diagonal line in the prediction. A lopsided pattern in the predicted response against the residuals response plots would have implied that the model is weak, which is not the case [2, 47]. The values of R^2 of 0.9956 for density, 0.9775 for hardness, and adjusted R^2 of 0.9879 for density, 0.9618 for hardness together with the residual analysis effectively fit the model to the experimental data.

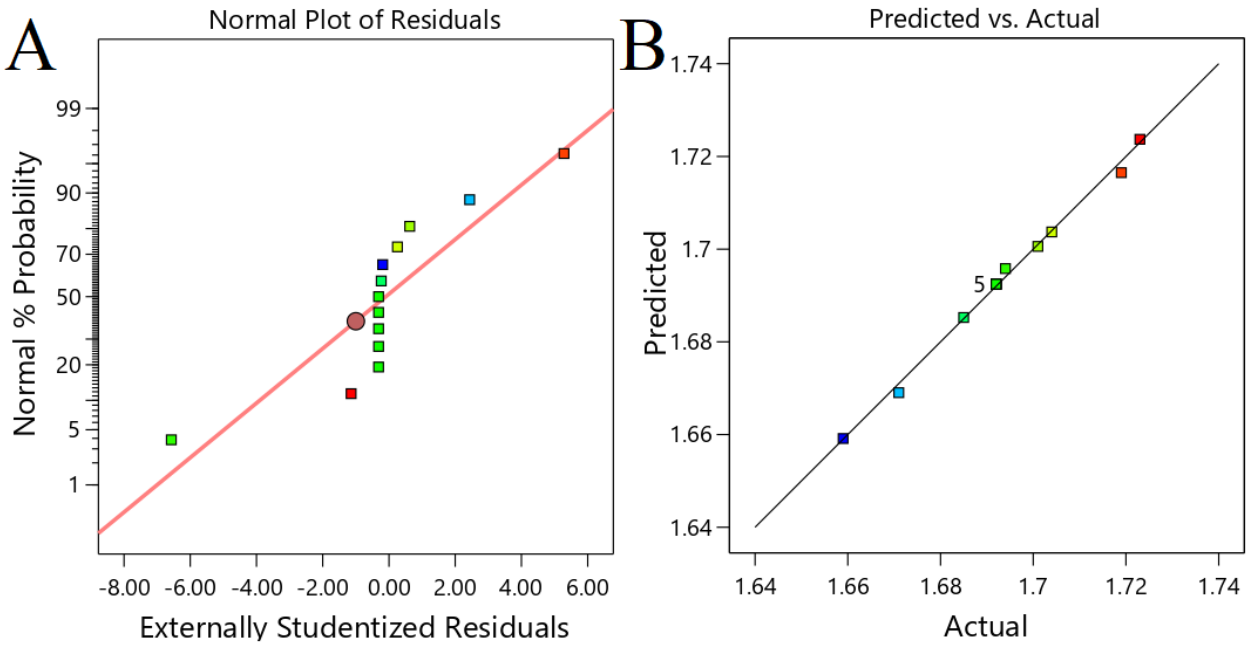

Figure 6. Stochastic error and a deterministic measure for the density of AZ91D-GNPs magnesium composites. (a) The normal probability plot of residuals, and (b) The predicted against actual values.

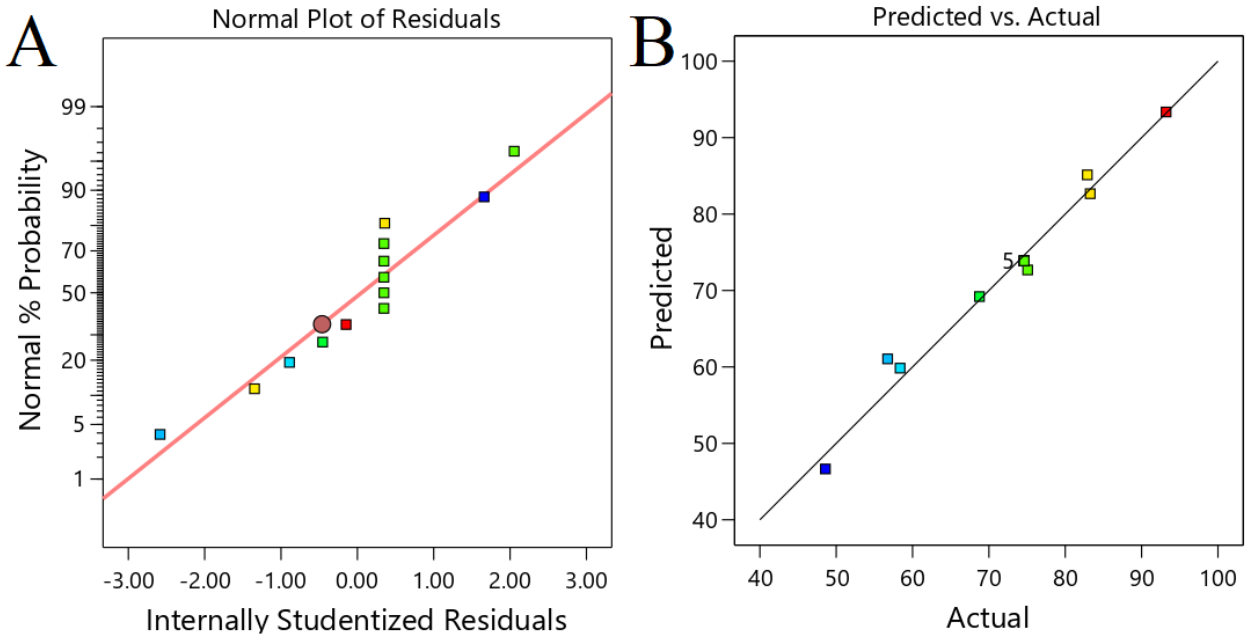

Figure 7. Stochastic error and a deterministic measure for the hardness of AZ91D-GNPs magnesium composites. (a) The normal probability plot of residuals, and (b) The predicted against actual values.

3.6. Interactive effect plots of density and hardness measurements

Figures 8 (a, b) and **9 (a, b)** shows the 2D contour and 3D plots for the interactive influence of pressure and temperature on the density and hardness of sintered AZ91D-Ni-GNPs composites. It could be observed that an increase in both sintering temperature and pressure results in an increase in the values of density and hardness. High sintering temperature and pressure result in lower densification and hardness values denoted by the blue colour area. It was apparent that the increment in sintering parameters such as temperature and pressure have a negative influence in improving the densification and hardness properties of the AZ91ZD-Ni-GNPs composites. As the sintering temperature and pressure increase, it could be observed that the densification and hardness values decrease gradually, moving from the red/green area to the blue area. The sintering temperature of 450 ℃ resulted in the highest density and hardness values of 1.723 g/cm3 and 93.21 HV, respectively (Table 3). Hence, the optimization focuses in terms of the factors used in this study is in the area where improved properties were obtained. This is the case in the study conducted by Chen et al. [2, 48]. In **Figures 10** and **11**, the plots of actual density and hardness values from the experimental study versus the RSM predicted density and hardness values of AZ91D-Ni-GNPs magnesium composite demonstrate minimal errors. It implies that the physical experimental values obtained substantially agree with the RSM predicted values from the model. This observation indicates that the developed model can adequately predict the density and hardness values of the AZ91D-Ni-GNPs composite.

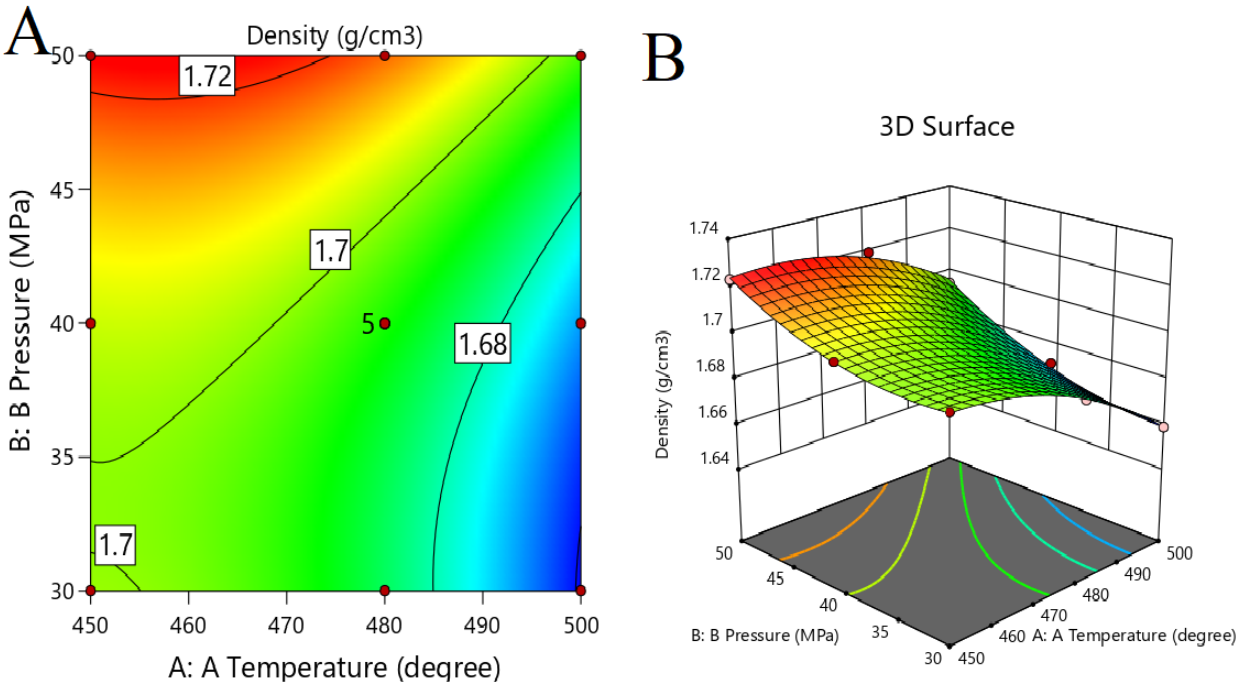

Figure 8. (a) The contour plots of the optimization results and (b) represent the 3D response surface plots showing the interaction effects between temperature and pressure on the density of SPS AZ91D-Ni-GNPs magnesium composites.

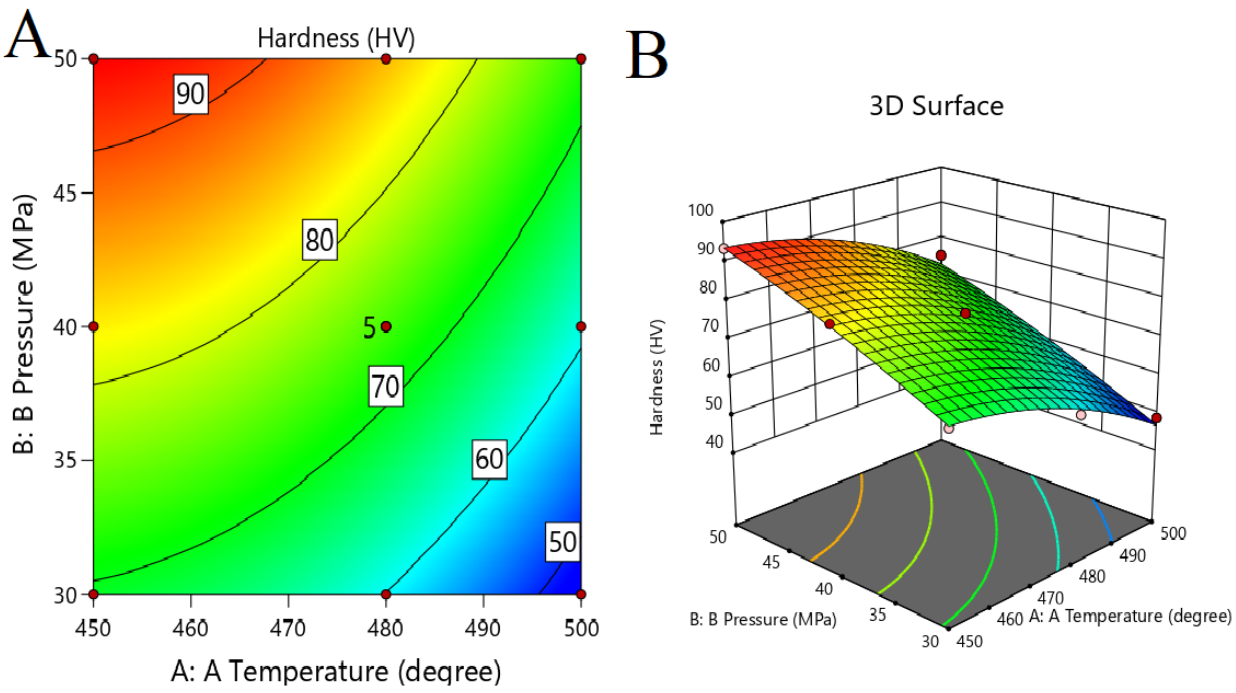

Figure 9. (a) The contour plots of the optimization results and (b) represent the 3D response surface plots showing the interaction effects between temperature and pressure on the density of SPS AZ91D-Ni-GNPs magnesium composites.

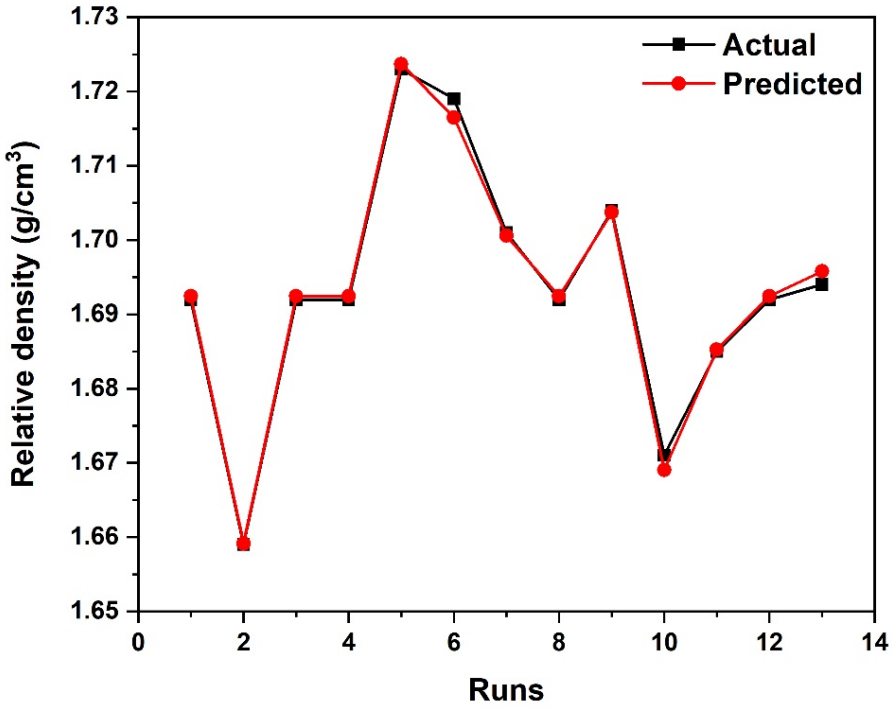

Figure 10. Actual relative density against the RSM predicted relative density of AZ91D-Ni-GNPs magnesium composite.

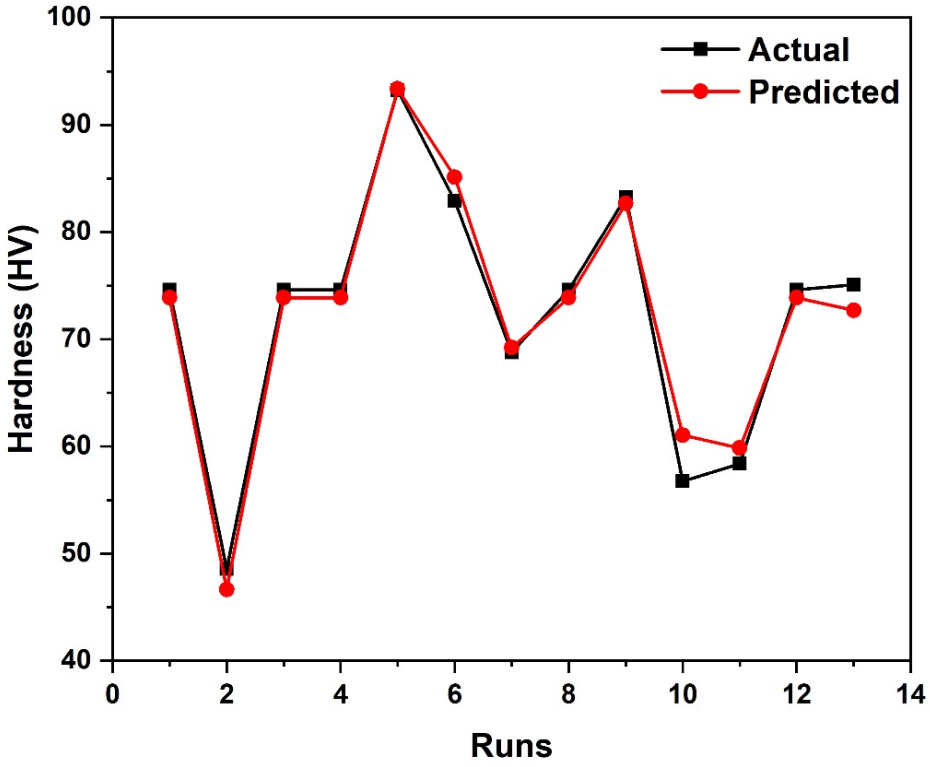

Figure 11. Actual hardness against the RSM predicted hardness of AZ91D-Ni-GNPs magnesium composite.

3.7. Validation studies of the density and hardness properties of AZ91D-Ni-GNPs composite

The adequacy of the models developed and acceptable optimal combination of variables was conducted using the design of expert software. This is necessary to establish the combination of factors that produce satisfactory responses (properties) [37]. Consequently, **Table 8** shows the twelve (12) optimal responses/solutions obtained through the optimization design. The SPS theory requires that materials be sintered at three-quarters (maximum safe sintering temperature) of their melting temperature for solid sintering. This serves as the constraint in selecting variables in this study [50]. Otherwise, a temperature beyond this threshold results in melt-out or liquid phase sintering. Typically, the desirability value for a given response ranges from 0 to 1, whereas an ideal case always presents a desirability value to be one (1). **Table 8** shows that the first 2 combinations of variables are the optimal combinations of factors (temperature and pressure) that produced better properties in terms of responses for sintered AZ91D-Ni-GNPs composite with desirability values that are approximately 1. The 12 solutions obtained indicate that the optimization study is ideal. In addition, **Figure 12** present the most suitable combination of variables that determine the best desirability range. This is determined based on the desirability value that is closest to 1, according to the design expert software analysis. Thus, the most suitable combination of factors comprises 450 ℃ sintering temperature and 50 MPa pressure with a corresponding density of 1.723 g/cm^3 and hardness of 93.24 HV.

Table 8. The Optimal combinations of density and hardness properties of AZ91D-Ni-GNPs magnesium-based composite.

Number	Temperature	Pressure	Density	Hardness	Desirability	
1	450.000	50.000	1.724	93.357	1.000	Selected
2	450.787	49.927	1.724	93.233	1.000	
3	450.541	49.941	1.724	93.264	0.999	
4	451.365	49.954	1.724	93.211	0.999	
5	451.015	49.994	1.724	93.278	0.997	
6	450.054	49.874	1.723	93.236	0.997	
7	450.258	49.911	1.724	93.257	0.996	
8	450.995	49.921	1.724	93.211	0.988	
9	451.700	49.992	1.724	93.217	0.988	
10	459.076	50.000	1.725	92.189	0.988	
11	459.409	50.000	1.725	92.124	0.988	
12	459.942	50.000	1.724	92.018	0.987	

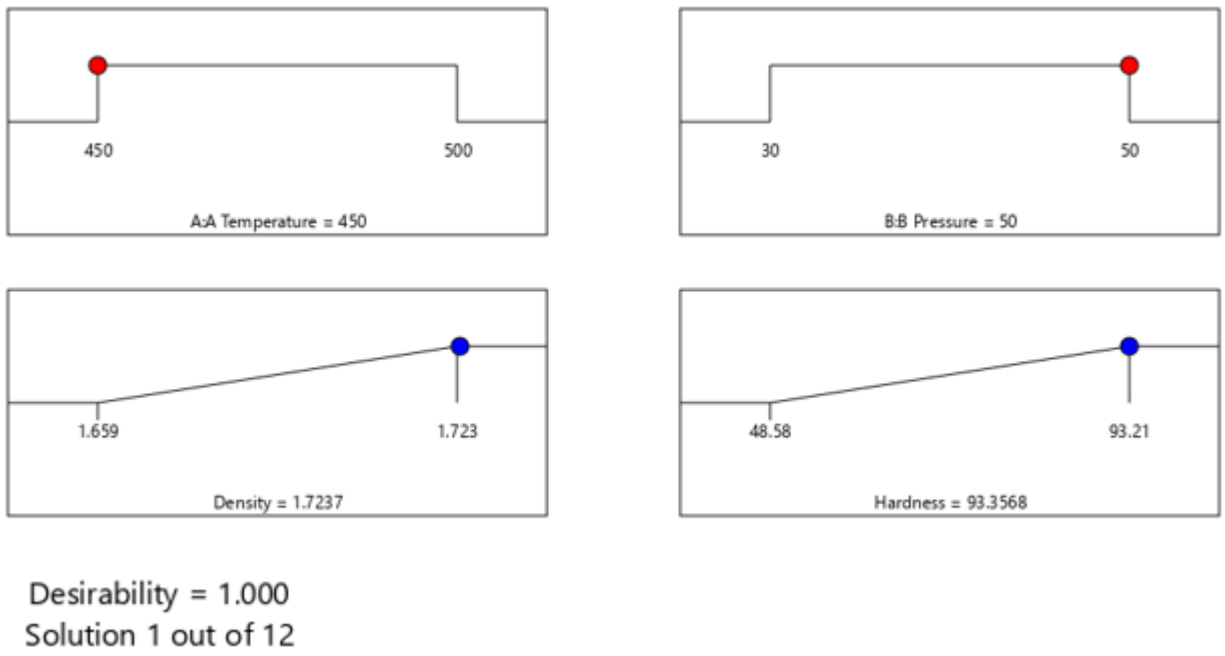

Figure 12. Desirability solution.

4. Microstructure analysis of AZ91D-Ni-GNPs composites

Synthesis of graphene nanoparticle (GNP), elemental nickel particle (Ni), and AZ91D magnesium alloy were successfully achieved by blending and SPS powder metallurgy method. **Figures 13** represent the optical micrographs of the sintered AZ91D-Ni-GNPs magnesium composite that possess optimal properties among the samples developed. **Figure 13a** represents the sample with the highest density and hardness properties with 1.723 g/cm^3 and 93.21HV, followed by **Figure 13b** with 1.719 and 83.27 HV, and **Figure 13c** with 1.704 g/cm^3 and 82.89 HV, respectively, in descending order. Subsequently, these three samples will be described as sample **A** (1.723 g/cm^3, 93.21 HV), **B** (1.719 g/cm^3, 83.27 HV, and **C** (1.704 g/cm^3, 82.89 HV). It is evident from the optical micrograph in **Figure 13 a-c** that minimal defects such as surface micro-cracks and micropores were present in the composites. Also, the interaction of the surface of the sample with the environment during metallography results in the formation of oxides observed in Figure 13 a-c. By comparing the sintered relative density and theoretical density, the relative densities obtained were greater than 97% density for samples A, B, and C, which implies that the sintering parameters used are appropriate in this study [43]. As reported by Zhu G. et al. [35], the combination of high sintering temperature and pressure is responsible for the high densification. Also, the initial spherical particle size of the AZ91D magnesium matrix is not evident in the sintered composites, rather the grain sizes were a mixture of different irregular shapes and the presence of few spherical grains. This development contributes to the improved densification and hardness properties of the sintered composites, thus, implying that SPS was able to induce high densification [51].

The grain boundaries were evident in the three selected samples, and the grain size increased with an increase in the sintering temperature. The average grain size for the three samples is in the range of 19 to 21 μm. Sample **A** has an average grain size of 19.73 μm, followed by sample **B** with an average grain size of 20.43 μm and sample **C** with 21.99 μm. Although, there is a marginal difference between the average value of the grain size for the three samples with nearly the same relative density, the increasing average grain size with increasing sintering temperature influence the hardness property of the composites. In the studies of Zhu Y. et al. [43], sintering temperature between 350 and 450 ℃ was used in the SPS of AZ91 magnesium alloy, and Minarik P et al. [52] used sintering temperature between 450 and 550 ℃ to develop AE42 magnesium alloy using SPS. They both reported that an increase in sintering temperature increases the average grain size in the sintered components, even with sintered materials having nearly the same relative density. They attributed it to the development of grain growth which reduced the formation of grain boundaries and subsequently the hardness property of the sintered components. The formation of grain size is a result of recrystallization along the initial particle boundaries (powder) of the matrix alloy [52] and recrystallization due to the inclusion of reinforcements (Ni and GNP) [4, 15] which serve as a catalyst for grain formation. The concurrent application of high sintering temperature and mechanical loading aids the formation of grains.

Additionally, the high statistical error results from varied character and dispersion of the grain size [52]. According to Minarik P. et al. [52], "the increment in the average grain size with the

increasing sintering temperature is systemic, but not statistically significant." The SEM and EDS analyses reveal more about the features of the sintered samples microstructures. **Figures 14a-c** illustrates the scanning electron microscopy (SEM) of the three selected samples, and **Figures 15a-i** present the X-ray spectroscopy (EDS) images of sample **A**. **Figure 15a** represent the micrograph of sample **A**, **Figure 15b** illustrates the mapping of all the elements present, and **Figures 15c-i** represent the mapping/dispersion of individual element present. From the SEM micrographs of the three samples selected (magnesium composite), the microstructural characteristics can be discussed in terms of: (a) dispersion of reinforcement and (b) surface morphology. It is evident from the three samples (SEM) selected that the grain shapes changed from the original spherical shape utilized for sintering to irregular shape in the sintered composites, and this validates the optical micrographs results. The changes indicate that sintering occurred through recrystallization, neck formation, and grain growth, which consequently lead to high densification. The large micropores formed at the contact points between two or more spherical particles disappeared during sintering [53], suggesting that the parameters used are appropriate for developing dense AZ91D-Ni-GNPs magnesium-based composites.

However, it can be observed from the SEM micrographs that the refinement of grains is not uniform in the microstructure, which might result from poor dispersion of reinforcement (two-dimensional GNPs) and temperature distribution in samples [19, 54]. Also, the few micropores observed were majorly present along the grain boundary and not within the grains in the three samples. The relative density measured through the Archimedes method revealed few micropores (>4%) in the selected samples. Although the percentage composition of reinforcements (Ni and GNP) are small (~3%), there were no traces of agglomeration or identifiable existence of periodic high-particle concentrated region within the grains and along the grain boundaries in the sintered samples. This implies that a good chemical bonding exists between the AZ91D magnesium alloys and Ni, GNPs reinforcements. While the EDS image reveals a trace of carbon, suggesting that the GNP was scantly distributed within the microstructure of the samples, this does not have a resemblance of an agglomerate. The sparse dispersion of nickel reinforcement (EDS) in the matrix alloy can be credited to its low percentage composition. The other trace element present in AZ91D magnesium alloy has minimal influence on the microstructure of the sintered composites.

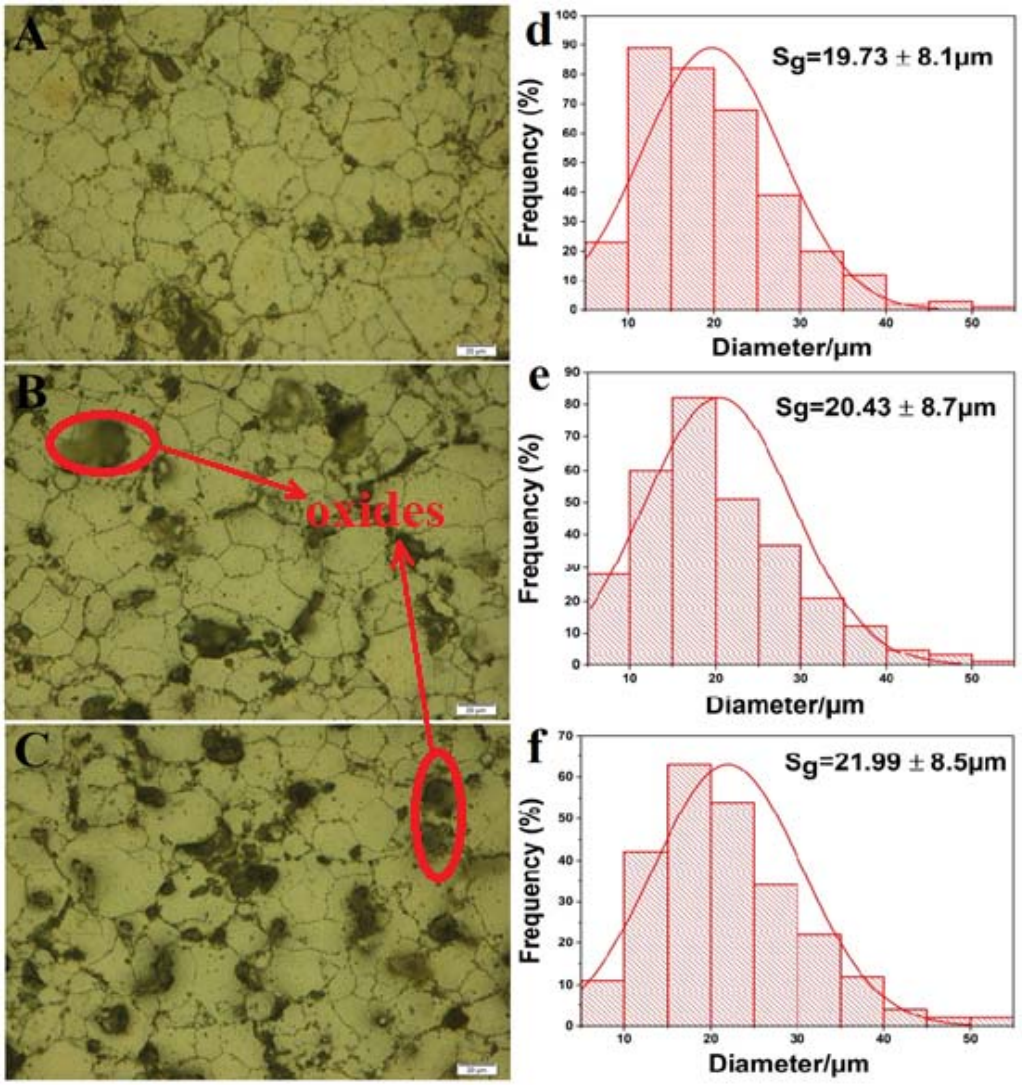

Figure 13. OM micrographs of AZ91D-Ni-GNPs magnesium composites. (a) 450℃, 50 MPa, (b) 450℃, 40 MPa, and (c) 480℃, 50 MPa, temperature, and pressure. (d-f) the distribution of the grain size.

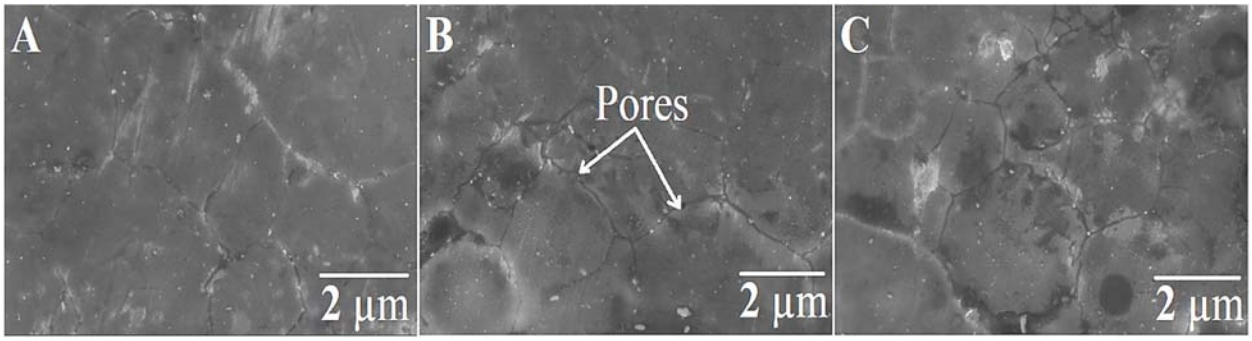

Figure 14. SEM images of AZ91D-Ni-GNPs magnesium composites. (a) 450℃, 50 MPa, (b) 450℃, 40 MPa, and (c) 480℃, 50 MPa, temperature, and pressure.

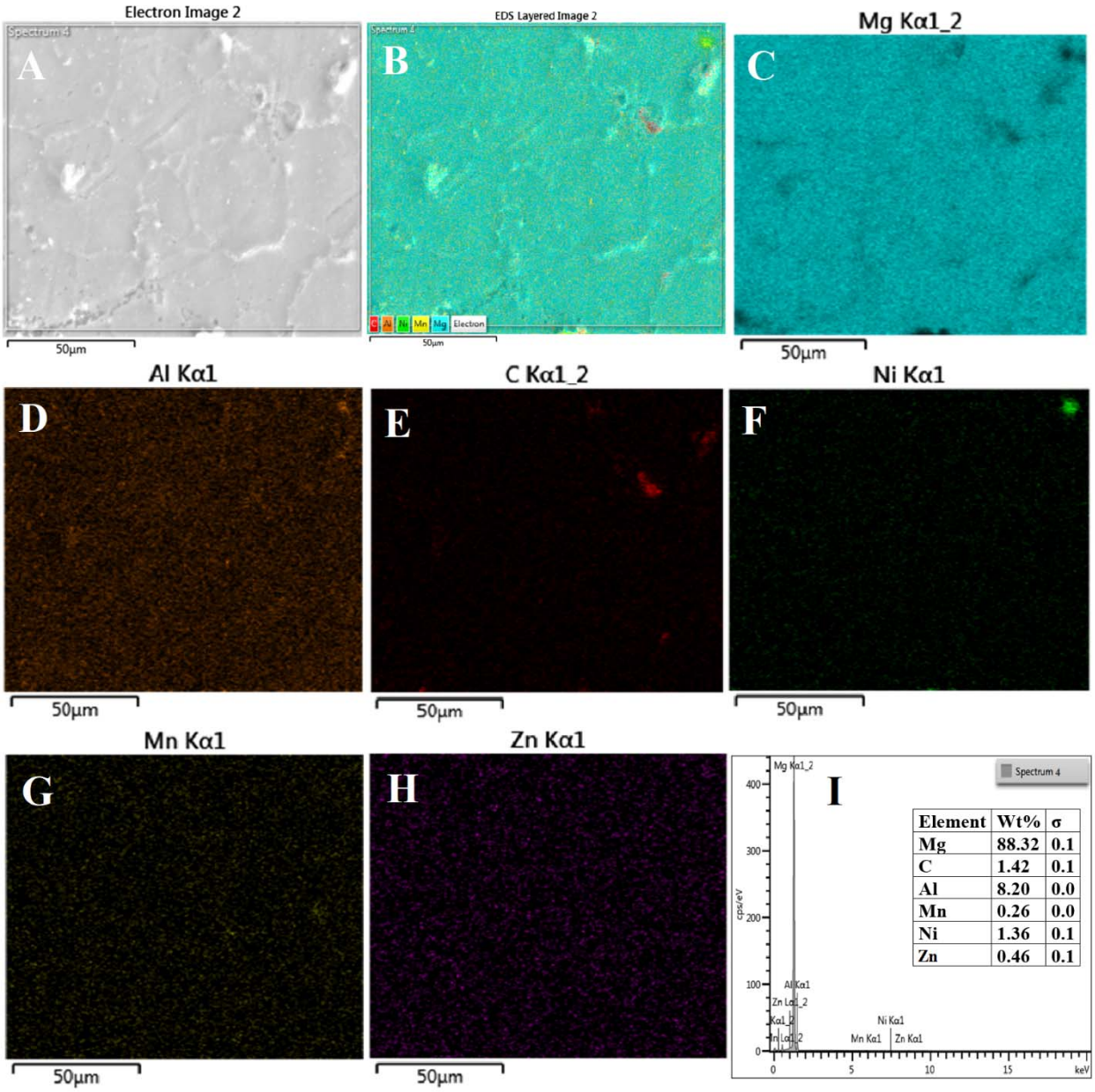

Figure 15. (a) EDS image of sample **A** (450℃, 50 MPa), (B) Elemental mapping (identifying the element present), (c) Magnesium, (d) Aluminium, (e) Carbon (f) Nickel, (g) Manganese, (h) Zinc, (i) EDS spectrum and the weight percent of the elements.

4.1. X-ray diffraction study of AZ91D-Ni-GNPs composites

The XRD patterns of the sintered AZ91D-Ni-GNPs magnesium composite processed at different sintering parameters denoted as sample A, B, C, and the XRD pattern of GNPs are shown in **Figure 16**. The XRD analysis of GNPs only shows a considerable peak at 2 theta = 26.4° angle of diffraction, which is not obvious in the sintered composites. However, the XRD analysis of the selected sintered composites (sample A, B, C) shows the presence of GNPs appearing as a minior peak at 2 theta = 77°. The EDS analysis corroborates the XRD result indicating the presence of

GNPs. The dominant phase from the XRD peaks of the sintered composite remains Mg matrix, while peaks representing the presence of GNPs, Ni, and $Mg_{17}Al_{12}$ are few. The major peaks of the Mg phase appear at 2 theta = 32.2°, 34.3°, 36.7°, 47.6°, 57.4°, 63.2°, 68.5°, and 70.0°, respectively, while the minor peaks appear at 2 theta = 74.9°, 78.9°, and 82.5°. In a similar study conducted by Sun X. et al.[1], the peaks obtained in the XRD analysis of graphene nanoplatelets reinforced magnesium composites are in agreement with the observation in this study. Thus, GNPs and Ni reinforcement in AZ91D alloy did not disrupt the formation of the Mg phase in the microstructure of spark plasma sintered AZ91D-Ni-GNPs composites. The major and minor peaks of Mg have hexagonal close-packed (HCP) structure with the major peaks corresponding to (100), (002), (101), (102), (110), (103), (112), and (201) planes of Mg. Additional peaks were not observed with the increase in sintering temperature. The only peak representing the presence of the Ni phase appears at 2 theta = 74.4° which corresponds to the (110) plane. In addition, a minor peak appears at 2 theta = 43° representing the $Mg_{17}Al_{12}$ phase. The intensity of this phase is small, and it is due to the low weight fraction of aluminium constituent present in the AZ91D alloy (corroborated by the EDS analysis) [43]. Although the presence of GNPs is slightly evident in the sintered composites, the Raman spectroscopy analysis was conducted further to establish the presence and behaviour of GNPs reinforcement.

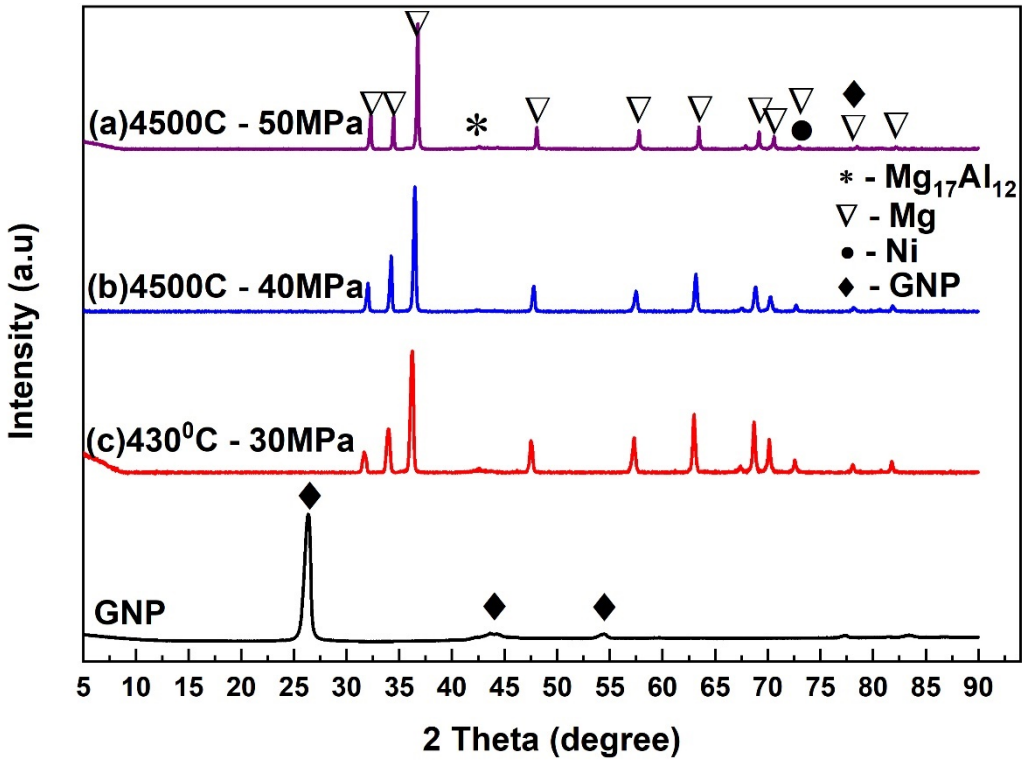

Figure 16. X-ray diffraction spectrum for AZ91D-Ni-GNPs magnesium composites. (a) 450℃, 50MPa, (b) 450℃, 40MPa, and (c) 480℃, 50MPa temperature and pressure.

4.2. Raman spectroscopy study of AZ91D-Ni-GNPs composites

The Raman spectra of the selected AZ91D-Ni-GNPs composites sintered at different sintering temperature is denoted as sample A, B, C and are shown in **Figure 17**. The Raman spectra obtained for sample A revealed two prominent peaks at 1346 cm^{-1} and 1591 cm^{-1}, which are related to the characteristics of the D band and G band [23]. A minor peak appears from sample B at 2696 cm^{-1}. This is associated with the characteristic of a 2D band **[21]**. The characteristic ratio of the intensity of D band to G band (I_D/I_G) explains the structural integrity or defect formation that occurs from the dispersion of GNPs in AZ91D/metal matrices [21]. Thus, the measurements of the I_D/I_G ratio of GNP for the three samples are 0.9, 1, 1.2. The increasing values imply the accumulation of non-sp^2 defects in the graphitic structure of GNPs when dispersing GNP in the metal matrix of AZ91D alloy. These defects (non-sp^2) that occur in the graphitic structure of carbon nanomaterials often present as broken edges and vacancies [23]. However, the measured value of I_D/I_G ratio of GNP in the AZ91D matrix for sample B and C are 1 and 1.2, indicating that less graphitization of carbon is formed during sintering. The 0.9 value of the I_D/I_G ratio of GNP in the AZ91D matrix suggests that the microstructure of the material is enhanced through the graphitization of GNPs during sintering. This signifies that the vacancies present in the microstructure are fill up and rearrange in their graphitic structure [23]**.** In addition, the observation in sample **A** suggest that magnesium atoms may have fill the pores in the structure of GNPs by infiltrating the carbon layers in the course of sintering, thus resulting in lower I_D/I_G value of 0.9 compared to 1 and 1.2 in sample **B** and **C**.

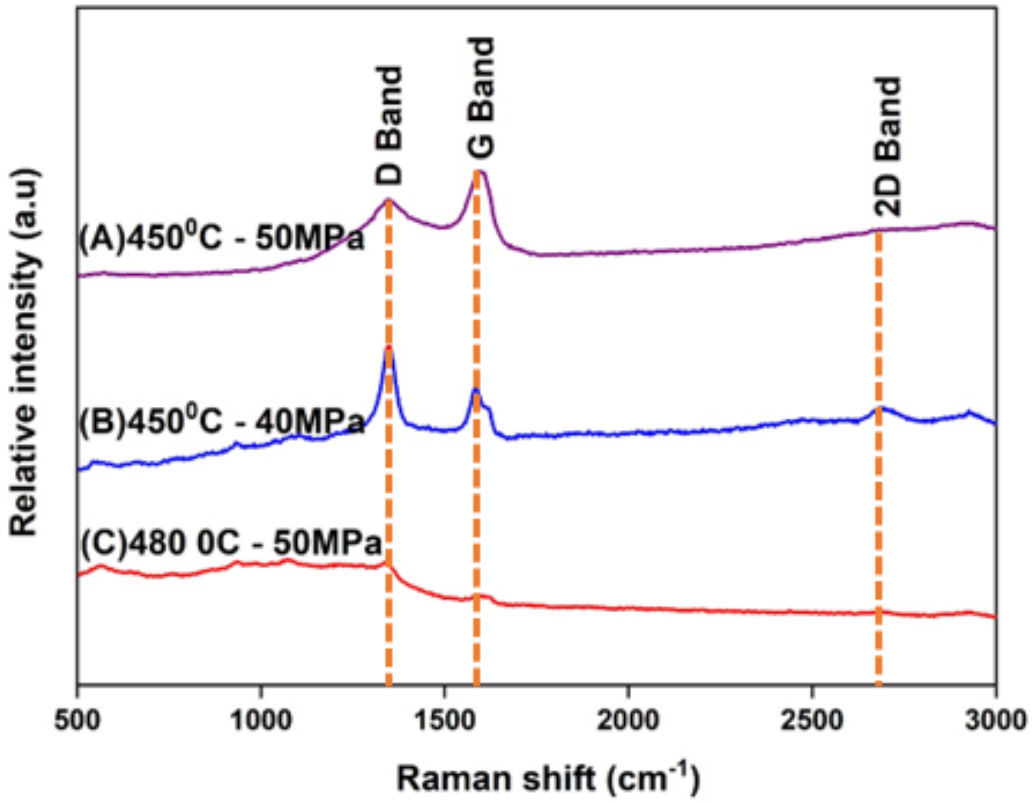

Figure 17. Raman spectra of AZ91D-Ni-GNPs magnesium composite. (a) 450 ℃, 50 MPa, (b) 450 ℃, 40 MPa, and (c) 480 ℃, 50 MPa temperature and pressure.

5. Conclusion

The study has explained the effect of the SPS process parameter variables on the synthesis, morphology, and properties of graphene nanoplatelets and nickel reinforced AZ91D magnesium alloy. This was investigated using RSM and CCD. Thus, the following conclusions are drawn based on the experimental results.

- RSM with central composite has been successfully deployed to formulate a statistical/mathematical model for predicting the density and hardness properties of AZ91D-Ni-GNPs magnesium-based composites by using the SPS technique.
- Within the range of this investigation, the experimental values of the density and hardness are reliable and in good form, with the empirical values for the two models, which are above 96% confidence levels. In addition, marginal and negligible errors were observed between the predicted and experimental values.
- The desirability analysis indicates that the optimum process parameters are 450 ℃ sintering temperature and 50 MPa pressure with the corresponding relative density of 1.723 g/cm^3 and 93.21 HV, respectively.

- The sintering temperature is the most effective parameter on the sintered AZ91D-Ni-GNPs composites, thus influencing the grain size formation.
- The process parameters are sufficient to produce AZ91D-Ni-GNPs magnesium-based composite with good morphology (reduced defects), dispersion of reinforcement, and metallurgical bonding.
- Thus, the optimization process removes the trials-by-error approach in the SPS manufacturing of AZ91D-Ni-GNPs magnesium-based composite and presents the interactive combination of process parameters clearly with their validities on the output. The ANOVA analyses obtained imply that the mathematical model from RSM-CCD is statistically adequate for this study.

Conflicts of interest

The authors declare that there are no conflicts of interest.

Acknowledgments

This work is funded by the Department of Chemical Engineering of the University of Pretoria and Faculty of Engineering, the Built Environment and Information Technology, Pretoria, South Africa.

Reference

[1] X. Sun, C. Li, X. Dai, L. Zhao, B. Li, H. Wang, C. Liang, H. Li and J. Fan, "Microstructures and properties of graphene-nanoplatelet-reinforced magnesium-matrix composites fabricated by an in situ reaction process," Journal of Alloys and Compounds, vol. 835, p. 155125, 2020.

[2] L. Chen, Y. Zhao, H. Hou, T. Zhang, J. Liang, M. Li and J. Li, "Development of AZ91D magnesium alloy-graphene nanoplatelets composites using thixomolding process," Journal of Alloys and Compounds, vol. 778, pp. 359-374, 2019.

[3] F. Pan, M. Yang, and X. Chen, "A review on casting magnesium alloys: modification of commercial alloys and development of new alloys," Journal of Materials Science & Technology, vol. 32, no. 12, pp. 1211-1221, 2016.

[4] S. F. Hassan, O. Nasirudeen, N. Al-Aqeeli, N. Saheb, F. Patel, and M. Baig, "Magnesium–nickel composite: Preparation, microstructure and mechanical properties," Journal of Alloys and Compounds, vol. 646, pp. 333-338, 2015.

[5] T. Zhang, Y. Zhao, L. Chen, J. Liang, M. Li, and H. Hou, "Graphene Nanoplatelets Reinforced Magnesium Matrix Composites Fabricated by Thixomolding," Acta Metall Sin, vol. 55, no. 5, pp. 638-646, 2019.

[6] O. N. Olalekan, M. Abdul Samad, S. F. Hassan, and M. M. I. Elhady, "Tribological evaluations of spark plasma sintered Mg–Ni composite," Tribology-Materials, Surfaces & Interfaces, pp. 1-9, 2021.

[7] Z. Taherian, V. S. Gharahshiran, A. Khataee, and Y. Orooji, "Synergistic effect of freeze-drying and promoters on the catalytic performance of Ni/MgAl layered double hydroxide," Fuel, vol. 311, p. 122620, 2022.

[8] Z. Taherian, A. Khataee, and Y. Orooji, "Facile synthesis of yttria-promoted nickel catalysts supported on MgO-MCM-41 for syngas production from greenhouse gases," Renewable and Sustainable Energy Reviews, vol. 134, p. 110130, 2020.
[9] Y. Huang, J. Li, L. Wan, X. Meng, and Y. Xie, "Strengthening and toughening mechanisms of CNTs/Mg-6Zn composites via friction stir processing," Materials Science and Engineering: A, vol. 732, pp. 205-211, 2018.
[10] K. Mathivanan, D. Thirumalaikumarasamy, M. Ashokkumar, S. Deepak, and M. Mathanbabu, "Optimization and prediction of AZ91D stellite-6 coated magnesium alloy using Box Behnken design and hybrid deep belief network," Journal of Materials Research and Technology, vol. 15, pp. 2953-2969, 2021.
[11] E. Ghasali, Y. Orooji, M. Alizadeh, and T. Ebadzadeh, "Chromium carbide, carbon nano tubes and carbon fibers reinforced magnesium matrix hybrid composites prepared by spark plasma sintering," Materials Science and Engineering: A, vol. 789, p. 139662, 2020.
[12] S. Arefi-Oskoui, A. Khataee, J. Behrouz Samira, V. Vatanpour, H. Gharamaleki Samira, Y. Orooji and M. Safarpour, "Development of MoS_2/O-MWCNTs/PES blended membrane for efficient removal of dyes, antibiotic, and protein," Separation and Purification Technology, vol. 280, p. 119822, 2022.
[13] M. Moussa, S. El-Hadad, and A. Nofal, "Influence of Si Addition on the Microstructure, Hardness and Elevated-Temperature Sliding Wear Behavior of AX53 Magnesium Alloy," International Journal of Metalcasting, pp. 1-14, 2021.
[14] S. K. Tiwari, S. Sahoo, N. Wang, and A. Huczko, "Graphene research and their outputs: Status and prospect," Journal of Science: Advanced Materials and Devices, vol. 5, no. 1, pp. 10-29, 2020.
[15] O. Ogunbiyi, R. Sadiku, O. Adesina, O. S. Adesina, S. Salifu, and J. Fayomi, "Microstructure and Mechanical Properties of Spark Plasma-Sintered Graphene-Reinforced Inconel 738 Low Carbon Superalloy," Metallurgical and Materials Transactions A, pp. 1-15, 2021.
[16] O. Ogunbiyi, T. Jamiru, R. Sadiku, O. Adesina, O. S. Adesina, and B. A. Obadele, "Spark plasma sintering of graphene-reinforced Inconel 738LC alloy: wear and corrosion performance," Metals and Materials International, pp. 1-15, 2020.
[17] M. Wang, Y. Zhao, Y. Zhu, X. Wang, J. Sheng, Z. Yang, H. Shi, Z. Shi and W. Fei, "Achieving high strength and ductility in graphene/magnesium composite via an in-situ reaction wetting process," Carbon, vol. 139, pp. 954-963, 2018.
[18] R. Zhao, J. Pei, W. Du, Z. Zhao, L. Zhang, J. Gao, P. Bai and D. Tie, "Fabrication of magnesium-coated graphene and its effect on the microstructure of reinforced AZ91 magnesium-matrix composites," Advanced Composites and Hybrid Materials, pp. 1-9, 2021.
[19] M. Rashad, F. Pan, A. Tang, M. Asif, and M. Aamir, "Synergetic effect of graphene nanoplatelets (GNPs) and multi-walled carbon nanotube (MW-CNTs) on mechanical properties of pure magnesium," Journal of Alloys and Compounds, vol. 603, pp. 111-118, 2014.
[20] F. Vahedi, A. Zarei-Hanzaki, A. Salandari-Rabori, A. Razaghian, H. Abedi, and P. Minarik, "Texture evolution and wear properties of a frictionally stir processed magnesium matrix composite reinforced by micro graphite and nano graphene particles," Materials Research Express, vol. 6, no. 10, p. 1065c6, 2019.

[21] K. Munir, C. Wen, and Y. Li, "Graphene nanoplatelets-reinforced magnesium metal matrix nanocomposites with superior mechanical and corrosion performance for biomedical applications," Journal of Magnesium and Alloys, vol. 8, no. 1, pp. 269-290, 2020.
[22] X. Du, W. Du, Z. Wang, K. Liu, and S. Li, "Defects in graphene nanoplatelets and their interface behavior to reinforce magnesium alloys," Applied Surface Science, vol. 484, pp. 414-423, 2019.
[23] M. Shahin, K. Munir, C. Wen, and Y. Li, "Magnesium-based composites reinforced with graphene nanoplatelets as biodegradable implant materials," Journal of Alloys and Compounds, vol. 828, p. 154461, 2020.
[24] M. Shahin, K. Munir, C. Wen, and Y. Li, "Nano-tribological behavior of graphene nanoplatelet–reinforced magnesium matrix nanocomposites," Journal of Magnesium and Alloys, vol. 9, no. 3, pp. 895-909, 2021.
[25] J. Alias, W. S. W. Harun, and H. M. Ayu, "A review on the preparation of magnesium-based alloys prepared by powder metallurgy and the evolution of microstructure and mechanical properties," in Key Engineering Materials, 2019, vol. 796: Trans Tech Publ, pp. 3-10.
[26] S. Jayasathyakawin, M. Ravichandran, N. Baskar, C. A. Chairman, and R. Balasundaram, "Magnesium matrix composite for biomedical applications through powder metallurgy–Review," Materials Today: Proceedings, vol. 27, pp. 736-741, 2020.
[27] W. Wong and M. Gupta, "Development of Mg/Cu nanocomposites using microwave assisted rapid sintering," Composites Science and Technology, vol. 67, no. 7-8, pp. 1541-1552, 2007.
[28] H. Fukuda, K. Kondoh, J. Umeda, and B. Fugetsu, "Aging behavior of the matrix of aluminum–magnesium–silicon alloy including carbon nanotubes," Materials Letters, vol. 65, no. 11, pp. 1723-1725, 2011.
[29] X. Sun, M. Chen, and D. Liu, "Fabrication and characterization of few-layer graphene oxide reinforced magnesium matrix composites," Materials Science and Engineering: A, vol. 803, p. 140722, 2021.
[30] O. Ogunbiyi, T. Jamiru, E. Sadiku, O. Adesina, L. Beneke, and T. Adegbola, "Spark plasma sintering of nickel and nickel based alloys: A Review," Procedia Manufacturing, vol. 35, pp. 1324-1329, 2019.
[31] Y. Orooji, A. Alizadeh, E. Ghasali, M. R. Derakhshandeh, M. Alizadeh, M. S. Asl and T. Ebadzadeh, "Co-reinforcing of mullite-TiN-CNT composites with ZrB_2 and TiB_2 compounds," Ceramics International, vol. 45, no. 16, pp. 20844-20854, 2019.
[32] Y. Orooji, A. Alizadeh, E. Ghasali, M. R. Derakhshandeh, M. Alizadeh, M. S. Asl and T. Ebadzadeh, "Co-reinforcing of mullite-TiN-CNT composites with ZrB_2 and TiB_2 compounds," Ceramics International, vol. 45, no. 16, pp. 20844-20854, 2019.
[33] Y. Orooji, M. R. Derakhshandeh, E. Ghasali, M. Alizadeh, M. S. Asl, and T. Ebadzadeh, "Effects of ZrB2 reinforcement on microstructure and mechanical properties of a spark plasma sintered mullite-CNT composite," Ceramics International, vol. 45, no. 13, pp. 16015-16021, 2019.
[34] X. Song, P. Zhang, P. Pei, J. Liu, R. Li, and G. Chen, "The role of spark plasma sintering on the improvement of hydrogen storage properties of Mg-based composites," International journal of hydrogen energy, vol. 35, no. 15, pp. 8080-8087, 2010.

[35] O. Ogunbiyi, T. Jamiru, E. Sadiku, L. Beneke, O. Adesina, and T. Adegbola, "Influence of sintering temperature on microstructural evolution of spark plasma sintered Inconel738LC," Procedia Manufacturing, vol. 35, pp. 1152-1157, 2019.
[36] M. Pahlavani, J. Marzbanrad, D. Rahmatabadi, R. Hashemi, and A. Bayati, "A comprehensive study on the effect of heat treatment on the fracture behaviors and structural properties of Mg-Li alloys using RSM," Materials Research Express, vol. 6, no. 7, p. 076554, 2019.
[37] M. Dada, P. Popoola, N. Mathe, S. Pityana, and S. Adeosun, "Parametric optimization of laser deposited high entropy alloys using response surface methodology (RSM)," The International Journal of Advanced Manufacturing Technology, vol. 109, no. 9, pp. 2719-2732, 2020.
[38] L. L. Soon, H. Zuhailawati, I. Suhaina, and B. K. Dhindaw, "Prediction of compressive strength of biodegradable Mg–Zn/HA composite via response surface methodology and its biodegradation," Acta Metallurgica Sinica (English Letters), vol. 29, no. 5, pp. 464-474, 2016.
[39] R. Soundararajan, A. Ramesh, N. Mohanraj, and N. Parthasarathi, "An investigation of material removal rate and surface roughness of squeeze casted A413 alloy on WEDM by multi response optimization using RSM," journal of alloys and compounds, vol. 685, pp. 533-545, 2016.
[40] A. Heidarzadeh and T. Saeid, "Correlation between process parameters, grain size and hardness of friction-stir-welded Cu–Zn alloys," Rare Metals, vol. 37, no. 5, pp. 388-398, 2018.
[41] R. Ghelich, M. R. Jahannama, H. Abdizadeh, F. S. Torknik, and M. R. Vaezi, "Central composite design (CCD)-Response surface methodology (RSM) of effective electrospinning parameters on PVP-B-Hf hybrid nanofibrous composites for synthesis of HfB2-based composite nanofibers," Composites Part B: Engineering, vol. 166, pp. 527-541, 2019.
[42] M. Mondet, E. Barraud, S. Lemonnier, J. Guyon, N. Allain, and T. Grosdidier, "Microstructure and mechanical properties of AZ91 magnesium alloy developed by Spark Plasma Sintering," Acta Materialia, vol. 119, pp. 55-67, 2016.
[43] Y. Zhu, J. Qin, J. Wang, and P. Jin, "Effect of sintering temperature on microstructure and mechanical properties of AZ91 magnesium alloy via spark plasma sintering," Advanced Engineering Materials.
[44] A. Oketola, T. Jamiru, A. T. Adegbola, O. Ogunbiyi, R. Sadiku, and S. Salifu, "Influence of sintering temperature on the microstructure, mechanical and tribological properties of ZrO2 reinforced spark plasma sintered Ni–Cr," International Journal of Lightweight Materials and Manufacture, vol. 5, no. 2, pp. 188-196, 2022.
[45] O. Ogunbiyi, E. Sadiku, T. Jamiru, O. Adesina, and L. Beneke, "Spark plasma sintering of Inconel 738LC: densification and microstructural characteristics," Materials Research Express, vol. 6, no. 10, p. 1065g8, 2019.
[46] O. Ogunbiyi, T. Jamiru, E. Sadiku, L. Beneke, O. Adesina, and T. Adegbola, "Microstructural characteristics and thermophysical properties of spark plasma sintered Inconel 738LC," The International Journal of Advanced Manufacturing Technology, vol. 104, no. 1-4, pp. 1425-1436, 2019.
[47] O. Ogunbiyi, T. Jamiru, R. Sadiku, O. Adesina, J. lolu Olajide, and L. Beneke, "Optimization of spark plasma sintering parameters of inconel 738LC alloy using response

surface methodology (RSM)," International Journal of Lightweight Materials and Manufacture, vol. 3, no. 2, pp. 177-188, 2020.
[48] L. Chen, Y. Zhao, M. Li, L. Li, L. Hou, and H. Hou, "Reinforced AZ91D magnesium alloy with thixomolding process facilitated dispersion of graphene nanoplatelets and enhanced interfacial interactions," Materials Science and Engineering: A, vol. 804, p. 140793, 2021.
[49] D. Guan, W. M. Rainforth, J. Sharp, J. Gao, and I. Todd, "On the use of cryomilling and spark plasma sintering to achieve high strength in a magnesium alloy," Journal of Alloys and Compounds, vol. 688, pp. 1141-1150, 2016.
[50] S. Jayasathyakawin, M. Ravichandran, N. Baskar, C. A. Chairman, and R. Balasundaram, "Mechanical properties and applications of Magnesium alloy–Review," Materials Today: Proceedings, vol. 27, pp. 909-913, 2020.
[51] P. Vijayakumar, K. Pazhanivel, N. Ramadoss, A. Ganeshkumar, K. Muruganantham, and M. Arivanandhan, "Synthesis and Characterization of AZ91D/SiC/BN Hybrid Magnesium Metal Matrix Composites," Silicon, pp. 1-11, 2022.
[52] P. Minarik, J. Stráský, J. Veselý, F. Lukáč, B. Hadzima, and R. Kral, "AE42 magnesium alloy prepared by spark plasma sintering," Journal of Alloys and Compounds, vol. 742, pp. 172-179, 2018.
[53] Y. Zhu, J. Qin, J. Wang, and P. Jin, "Effect of sintering temperature on microstructure and mechanical properties of AZ91 magnesium alloy via spark plasma sintering," Advanced Engineering Materials, p. 2100905, 2021.
[54] W. N. A. W. Muhammad, Z. Sajuri, Y. Mutoh, and Y. Miyashita, "Microstructure and mechanical properties of magnesium composites prepared by spark plasma sintering technology," Journal of Alloys and Compounds, vol. 509, no. 20, pp. 6021-6029, 2011.